

Kernel Two-Sample Tests for Manifold Data

Xiuyuan Cheng* Yao Xie†

Abstract

We present a study of a kernel-based two-sample test statistic related to the Maximum Mean Discrepancy (MMD) in the manifold data setting, assuming that high-dimensional observations are close to a low-dimensional manifold. We characterize the test level and power in relation to the kernel bandwidth, the number of samples, and the intrinsic dimensionality of the manifold. Specifically, when data densities p and q are supported on a d -dimensional sub-manifold \mathcal{M} embedded in an m -dimensional space and are Hölder with order β (up to 2) on \mathcal{M} , we prove a guarantee of the test power for finite sample size n that exceeds a threshold depending on d , β , and Δ_2 the squared L^2 -divergence between p and q on the manifold, and with a properly chosen kernel bandwidth γ . For small density departures, we show that with large n they can be detected by the kernel test when Δ_2 is greater than $n^{-2\beta/(d+4\beta)}$ up to a certain constant and γ scales as $n^{-1/(d+4\beta)}$. The analysis extends to cases where the manifold has a boundary and the data samples contain high-dimensional additive noise. Our results indicate that the kernel two-sample test has no curse-of-dimensionality when the data lie on or near a low-dimensional manifold. We validate our theory and the properties of the kernel test for manifold data through a series of numerical experiments.

Keywords: Kernel methods, manifold data, Maximum Mean Discrepancy, two-sample test.

1 Introduction

Two-sample testing aims to determine whether two sets of samples are drawn from the same distribution. In the classical setting, given two independent sets of data in \mathbb{R}^m ,

$$x_i \sim p, i = 1, \dots, n_X, \text{ i.i.d.}, \quad y_j \sim q, j = 1, \dots, n_Y, \text{ i.i.d.}, \quad (1)$$

the two-sample problem seeks to accept or reject the null hypothesis $H_0 : p = q$. Here, we assume the data follow distributions with densities p and q , respectively. It is also of practical interest to identify where $p \neq q$ when the two distributions differ. The problem is fundamental in statistics and signal processing with broad applications in scientific discovery and machine learning. Exemplar applications include anomaly detection [13, 14, 6], change-point detection [66, 12, 65], differential analysis of single-cell data [68], model criticism [41, 19, 7], general data analysis of biomedical data, audio and imaging data [8, 20, 36, 16], and machine learning applications [39, 41, 59, 19, 37, 42].

As an example of application in machine learning, suppose we are interested in performing an out-of-distribution (OOD) test [52] to determine whether or not the new incoming testing batch of data samples follows the same distribution as the training samples. If the distribution is significantly different, re-training the model to adapt to the new data distribution may be required, or the batch will be labeled as OOD. In performing such a task, we are to compare the two sets of samples from training and the new

*Department of Mathematics, Duke University. Email: xiuyuan.cheng@duke.edu

†H. Milton Stewart School of Industrial and Systems Engineering, Georgia Institute of Technology. Email: yao.xie@isye.gatech.edu.

arrival batch and determine whether (and how) their distributions differ. When data have low-dimensional structures, it is important to consider the data geometry in the OOD test.

In many applications, high-dimensional real data have intrinsically low-dimensional structures such as manifolds. For example, it is known that patches of natural images lie on sub-manifolds in the pixel space [10, 47], and so do image features extracted by deep neural networks [54, 69]. Another example is the single-cell RNA sequencing data where measurements lie near to curve-like structures due to the time development of cells, known as the “cell trajectory” [62, 53]. For natural images, a simple dataset is the MNIST hand-written digits (illustrated in Example 1 and Figure 2), which is one of the most commonly used datasets in statistics and machine learning research. Although the original MNIST data is not exactly on the manifold, they can be viewed as having approximately manifold-like structures. In Example 1, we provide a case where high dimensional image data lie exactly on a smooth manifold by simulating rotated copies of the same digit image for illustrative purposes. In this work, we consider the manifold data setting where distributions p and q are supported on (or near to) a d -dimensional manifold \mathcal{M} embedded in \mathbb{R}^m , with $d \leq m$. We refer to \mathbb{R}^m as the ambient space and d as the intrinsic dimensionality of the manifold data.

Traditional statistical methods for two-sample testing have focused on parametric or low-dimensional testing scenarios, such as Hotelling’s two-sample test [34] and Student’s t-test [48]. When it is challenging to specify the exact parametric form of the distributions, non-parametric two-sample tests are more suitable. Earlier works on one-dimensional non-parametric two-sample tests are based on the Kolmogorov-Smirnov distance [49, 43], the total variation distance [29], among others. Extending these tests to high-dimensional data is non-trivial.

Modern non-parametric tests for high-dimensional data have been developed, many based on integral probability metrics [58]. A notable contribution is the Reproducing Kernel Hilbert Space (RKHS) kernel Maximum Mean Discrepancy (MMD) two-sample test [28, 27], which is related to U-statistics [55]. The asymptotic optimality of kernel MMD tests was recently studied in [2, 40]. Wasserstein distance two-sample tests have been considered in [22, 50], and graph-based statistics have been proposed for distribution-free tests in high dimensions [15, 5].

However, it is known that non-parametric two-sample tests face difficulties with high-dimensional data. For instance, [51] provided a negative result for kernel MMD in high dimension that the test power decreases may decrease polynomially with increasing data dimension when applied to detect the mean shift of Gaussian distributions. However, the argument therein does not consider possible intrinsically low-dimensional structures of high-dimensional data. Furthermore, we also observe that the roles of the kernel bandwidth and the data dimensionality were not explicitly specified in the original kernel MMD test paper [27], both of which may play a crucial role in determining the performance of the kernel test in practice.

In this paper, we aim to answer the following fundamental questions about kernel tests applied to high-dimensional data with intrinsically low-dimensional structure:

Question 1. *Will a decrease in test power be observed as data dimension increases when the data has intrinsic low-dimensionality such as lying on sub-manifolds?*

Question 2. *When using kernel tests on manifold data, how should one select the kernel bandwidth, given that it often significantly impacts the performance of kernel methods?*

We provide a positive answer to Question 1 by providing a non-asymptotic result. Theoretically, we show that when data densities are supported on a d -dimensional sub-manifold \mathcal{M} embedded in \mathbb{R}^m (clean manifold data with no noise), the kernel two-sample test achieves a positive test power (at the specified test level) when the number of samples n exceeds a certain threshold depending on the manifold dimension d , the squared L^2 -divergence $\Delta_2(p, q)$ between the two distributions on \mathcal{M} , the Hölder regularity β of densities defined with respect to the intrinsic manifold distance, among other intrinsically defined quantities and with a properly chosen kernel bandwidth γ (Theorem 3.5). This finite-sample result gives that, with large

n , a small departure of q from p can be detected by the kernel test when Δ_2 exceeds $n^{-2\beta/(d+4\beta)}$ up to a certain constant (Corollary 3.6). In addition, to achieve test consistency under this regime, the kernel bandwidth γ needs to scale as $n^{-1/(d+4\beta)}$. This provides a theoretical answer to Question 2 for detecting a possibly small density departure given finite samples.

The above result holds for densities p and q in the Hölder class $\mathcal{H}^\beta(\mathcal{M})$, $0 < \beta \leq 2$. When higher order regularity of p and q presents, it no longer improves the theoretical rate (see Remark 3.3). Our finite-sample analysis shows that the properties of the kernel test are only affected by the intrinsic dimensionality d rather than the ambient dimensionality m . In our result, the definitions of the quantities d , Δ_2 and β are all intrinsic to the manifold geometry (see more in Section 2.3), while any characterization through kernel spectrum would be non-intrinsic at finite kernel bandwidth.

Our result indicates that kernel tests can avoid the curse of dimensionality for manifold data, which is consistent with a similar result for kernel density estimation in [45]. When the kernel is positive semi-definite (PSD), the kernel test we study equals the RKHS kernel MMD statistic [27]. However, our analysis also covers non-PSD kernels, where the technical requirement for the kernel function is regularity, decay, and positivity, as stated in Assumption 3.3. Our theory suggests that a larger class of kernel tests that is MMD-like but more general than MMD can have test power. This opens the possibility of constructing more general kernels for testing problems in practice. In Section 5.3, we provide experimental evidence demonstrating the testing power with non-PSD kernels.

Our result can also be connected to two-sample tests for Functional Data Analysis [33] where data samples are (discretized) functions. In fact, our Example 1 of image data lying on a manifold also happens to be a case of vector data having underlying functional limits (the image dimensionality increases with finer resolution). It was shown in [64] that when the kernel bandwidth is properly scaled, kernel MMD tests for functional data can retain power on high dimensional data by converging to a limiting kernel test over functions. This leads to the same positive answer of kernel tests in high dimension with our result but is from a different perspective. The underlying functional limit can be interpreted as effectively a low dimensionality of the data and a special case of data lying on (hidden) manifolds. The Riemannian manifold data considered in this work is a more general framework for the intrinsic low-dimensionality of vector data (for cases beyond those like Example 1), and the functional data setting extends to broader cases of non-vector data, e.g., functions evaluated on un-shared meshes. Notably, our result also indicates that a proper choice of kernel bandwidth is important for testing performance, where the optimal choice is not always the median distance heuristic.

We begin by proving the consistency of the kernel test when the data densities lie on a smooth manifold without a boundary. We then extend the theory to submanifolds with a smooth boundary. The manifold with boundary setting includes, as a special case, the Euclidean data case, where p and q are supported on a compact domain in \mathbb{R}^m with a smooth boundary, and $d = m$. The theory also extends to the case where manifold data are corrupted by additive Gaussian noise in the ambient space \mathbb{R}^m . We show, theoretically, that as long as the coordinate-wise Gaussian noise level σ is less than γ/\sqrt{m} up to an absolute constant (γ being the kernel bandwidth parameter), the kernel tests computed from noisy data have the same theoretical consistency rate as clean data lying on the manifold. In this case, the test consistency is determined only by the pair of two densities of the clean manifold data.

Our experiments demonstrate that the test power can be maintained (for fixed test level) as the ambient dimensionality m increases for low-dimensional manifold data embedded in high-dimensional space. Specifically, we construct an example of group-transformed images with increasingly refined resolution (i.e., increasing image size). We also conduct experiments on noise-corrupted data. In the theoretical regime of small additive noise, the performance of kernel tests on noisy data is similar to that on clean data, as predicted by the theory. Next, we apply kernel tests to the more complicated hand-written digits data set, which no longer lies exactly on manifolds. We demonstrate that kernel bandwidth much smaller than the median distance bandwidth can provide better performance. Finally, we numerically show that non-PSD kernels that may or may not satisfy the proposed theoretical conditions can provide a kernel test with power.

Table 1: List of default notations

m	dimensionality of the ambient space	β	Hölder class $\mathcal{H}^\beta(\mathcal{M})$
d	intrinsic dimensionality of the manifold	L_ρ	Upper bound of Hölder constants (defined in Section 3.1) of p and q on \mathcal{M}
\mathcal{M}	d -dimensional manifold in \mathbb{R}^m	ρ_{\max}	Uniform upper bound of p and q on \mathcal{M}
dV	volume form on \mathcal{M}	γ	kernel bandwidth parameter
$d_{\mathcal{M}}(x, y)$	manifold geodesic distance	K_γ	kernel applied to data, $K_\gamma(x, y) = h\left(\frac{\ x-y\ ^2}{\gamma^2}\right)$
$\ x - y\ $	Euclidean distance in \mathbb{R}^m	h	C^1 and decay function on $[0, \infty)$, $h \geq 0$
p, q	data sampling densities on \mathcal{M}	m_0	$m_0[h] := \int_{\mathbb{R}^d} h(u ^2) du$
n_X, n_Y	number of samples in two-sample datasets X and Y respectively	Asymptotic Notations	
n	$n = n_X + n_Y$	$O(\cdot)$	$f = O(g)$: there exists $C > 0$ such that when $ g $ is sufficiently small, $ f \leq C g $.
ρ_X	$n_X/n \rightarrow \rho_X$	$O_x(\cdot)$	declaring the constant dependence on x .
\hat{T}	empirical kernel statistic (2)		
T	population kernel statistic (7)		

Our work adopts analytical techniques from the geometrical data analysis and manifold learning literature, particularly the analysis of local kernels on manifolds from [21]. As a quick recap of related works: seminal works such as [3, 4, 30, 21] have demonstrated that the graph diffusion process on a kernelized affinity graph constructed from high-dimensional data vectors converges to a continuous diffusion process on the manifold as the sample size increases to infinity and the kernel bandwidth decreases to zero. The results in [57] and subsequent works demonstrate the approximation error to the manifold diffusion operator at a finite sample size, where the sample complexity only involves the intrinsic dimensionality. Another line of related works concerns the spectral convergence of kernel matrices constructed from manifold data. Note that the kernel function itself is computed from Euclidean coordinates of data in \mathbb{R}^m and thus extrinsic. Therefore, any theoretical properties involving the kernel spectrum are also non-intrinsic to the manifold. In the limit of kernel bandwidth going to zero, the spectrum of kernelized graph Laplacian matrices has been shown to converge to that of the manifold Laplacian operator [61, 11, 24, 18]. However, bounding the difference between the extrinsic kernel spectrum to the intrinsic limiting spectrum incurs more complicated analysis under additional assumptions. Our work addresses this limit by revealing the limiting population kernel MMD-like statistic as the squared L^2 divergence up to a constant scaling factor (Lemma 3.2), which is a simpler analysis.

In the rest of the paper, the necessary preliminaries and notations are provided in Section 2. In Section 3, we present the theory for kernel tests on manifold data and establish the consistency and power of the test. We then extend this theory to cover the case of a manifold with boundary and data containing high-dimensional noise in Section 4. Numerical experiments are presented in Section 5, and we discuss potential future research directions in Section 6. All proofs are provided in Appendix A.

2 Preliminaries

Following the setup in (1), we define $n := n_X + n_Y$. We also assume that n_X and n_Y are proportional, that is, as n increases, n_X/n approaches a constant $\rho_X \in (0, 1)$. As our non-asymptotic analysis will consider a finite n , the constant proportion will be reflected in a “balancing” condition, see (11).

2.1 Classical RKHS kernel MMD statistic

The (biased) empirical estimate for the squared kernel MMD statistic [27] is defined as

$$\hat{T} := \frac{1}{n_X^2} \sum_{i,i'=1}^{n_X} K_\gamma(x_i, x_{i'}) + \frac{1}{n_Y^2} \sum_{j,j'=1}^{n_Y} K_\gamma(y_j, y_{j'}) - \frac{2}{n_X n_Y} \sum_{i=1}^{n_X} \sum_{j=1}^{n_Y} K_\gamma(x_i, y_j), \quad (2)$$

where $K_\gamma(x, y)$ is a PSD kernel with a user-specified *bandwidth* parameter $\gamma > 0$. The corresponding population statistic T will be given in (7) below.

We consider a kernel with a fixed bandwidth, that is,

$$K_\gamma(x, y) = h\left(\frac{\|x - y\|^2}{\gamma^2}\right), \quad h : [0, \infty) \rightarrow \mathbb{R}, \quad (3)$$

where h usually is some non-negative function. A standard example is the Gaussian radial basis function (RBF) kernel, defined by $h(r) = \exp(-r/2)$. The classical theory of kernel MMD tests requires the kernel to be characteristic, ensuring that the MMD distance is a metric between distributions [27]. However, in this paper, we relax this assumption and only require h to be a non-negative, C^1 function that decays, which does not necessarily lead to a positive semi-definite (PSD) kernel K_γ . Please refer to Assumption 3.3 and the subsequent comments for further discussion.

The unbiased estimator of the kernel MMD removes the diagonal entries $K(x_i, x_i)$ and $K(y_j, y_j)$ in the summation in (2), and has a slightly different normalization (by $1/(N(N-1))$ rather than $1/N^2$, where $N = n_X$ and n_Y respectively). Since diagonal entries always equal $h(0)$, which is a constant, the biased and unbiased estimators give the same behavior in our setting qualitatively. In this paper, we focus on the biased estimator (2), and the analysis can be extended to the unbiased estimator.

2.2 Test level and power

We adopt the standard statistical definitions [27] for the test level α_{level} and testing power. In the two-sample test setting, one computes the kernel test statistic \hat{T} from datasets X and Y and chooses a threshold t_{thres} . If $\hat{T} > t_{\text{thres}}$, the test rejects the null hypothesis H_0 .

The ‘‘level’’ of a test, denoted by α_{level} , is the target Type-I error. A test achieves a level α_{level} if

$$\mathbb{P}[\hat{T} > t_{\text{thres}} | H_0] \leq \alpha_{\text{level}}, \quad (4)$$

where $0 < \alpha_{\text{level}} < 1$ is typically set to a small constant, such as $\alpha_{\text{level}} = 0.05$. To control the Type-I error (4), the threshold t_{thres} needs to exceed the $(1 - \alpha_{\text{level}})$ -quantile of the distribution of \hat{T} under H_0 . Typical asymptotic theory determines t_{thres} by the limiting distribution of the detection statistic \hat{T} under H_0 , which is a χ^2 distribution in many cases. However, the distribution of \hat{T} may significantly differ from the limiting distribution at a finite sample size. In practice, t_{thres} is usually estimated using a standard bootstrap procedure [27, 31].

The Type-II error of the statistic \hat{T} and the threshold t_{thres} is given by $\mathbb{P}[\hat{T} \leq t_{\text{thres}} | H_1]$ under the alternative hypothesis. The *testing power* (at level α_{level}) corresponds to one minus the Type-II error. The test is said to be *asymptotically consistent* if the testing power can approach 1 as the sample size n increases. In this work, we will characterize the testing power of the kernel test at a finite sample size.

2.3 Riemannian manifold and intrinsic geometry

The differential geometric notations employed in this paper are standard and can be found in, for example, [23]. We consider a smooth connected manifold \mathcal{M} of dimension d equipped with a Riemannian metric tensor $g_{\mathcal{M}}$. The manifold \mathcal{M} is isometrically embedded in the Euclidean space \mathbb{R}^m , where m is the ambient

dimension and can be much larger than the intrinsic dimension d . Let $\iota : \mathcal{M} \rightarrow \mathbb{R}^m$ be the C^∞ isometric embedding, and let $\iota(x) \in \mathbb{R}^m$ denote the extrinsic coordinates. In this paper, we use the same notation x to represent both a point $x \in \mathcal{M}$ and its image $\iota(x) \in \mathbb{R}^m$, provided that there is no ambiguity. Note that different embeddings in different spaces can be associated with the same Riemannian manifold $(\mathcal{M}, g_{\mathcal{M}})$. A quantity is called *intrinsic* if it solely depends on $g_{\mathcal{M}}$ and is independent of the embedding or extrinsic coordinates.

Given the Riemannian metric $g_{\mathcal{M}}$, the geodesic distance can be defined at least locally. We assume that the geodesic distance $d_{\mathcal{M}}(x, y)$ is globally defined on \mathcal{M} and induces a metric on \mathcal{M} . This is possible when \mathcal{M} is also compact, and in this case, $d_{\mathcal{M}}$ coincides with the Riemannian distance, and every two points on \mathcal{M} are joined by a length minimizing geodesic. The Euclidean distance in \mathbb{R}^m is denoted by $\|x - y\|$. The manifold differential operators are defined intrinsically with respect to $g_{\mathcal{M}}$. For instance, for a C^1 function f on \mathcal{M} , $\nabla_{\mathcal{M}}f(x)$ denotes the manifold gradient of f at point x , which consists of partial derivatives with respect to the normal coordinates. The Hölder class $\mathcal{H}^\beta(\mathcal{M})$ is defined with respect to manifold geodesic distance, and in this work, we consider $0 < \beta \leq 2$. Specifically,

(i) When $\beta \leq 1$,

$$\mathcal{H}^\beta(\mathcal{M}) = \{f \in C^0(\mathcal{M}), \exists L > 0, |f(x) - f(y)| \leq Ld_{\mathcal{M}}(x, y)^\beta, \forall x, y \in \mathcal{M}\},$$

and we define the *Hölder constant* of f as $L_f := \sup_{x \neq y \in \mathcal{M}} |f(x) - f(y)|/d_{\mathcal{M}}(x, y)^\beta$.

(ii) When $1 < \beta \leq 2$,

$$\mathcal{H}^\beta(\mathcal{M}) = \{f \in C^1(\mathcal{M}), \exists L > 0, \|\nabla_{\mathcal{M}}f(x) - \nabla_{\mathcal{M}}f(y)\| \leq Ld_{\mathcal{M}}(x, y)^{\beta-1}, \forall x, y \in \mathcal{M}\},$$

and then we define $L_f := \|\nabla_{\mathcal{M}}f\|_\infty + \sup_{x \neq y \in \mathcal{M}} \|\nabla_{\mathcal{M}}f(x) - \nabla_{\mathcal{M}}f(y)\|/d_{\mathcal{M}}(x, y)^{\beta-1}$.

Because $\nabla_{\mathcal{M}}f(x)$ is a cotangent vector at x , the formal definition of $\|\nabla_{\mathcal{M}}f(x) - \nabla_{\mathcal{M}}f(y)\|$ utilizes the parallel transport $P_{y,x}$ along the geodesic from x to y . (For any tangent vector $v \in T_x\mathcal{M}$, $P_{y,x}v \in T_y\mathcal{M}$ and preserves the length under $g_{\mathcal{M}}$.) Specifically, $\|\nabla_{\mathcal{M}}f(x) - \nabla_{\mathcal{M}}f(y)\| = \sup_{v \in T_x\mathcal{M}, \|v\|=1} |\nabla_{\mathcal{M}}f(x)(v) - \nabla_{\mathcal{M}}f(y)(P_{y,x}v)|$. Our notion of the Hölder constant L_f removes the C^0 norm $\|f\|_\infty$ from the usual definition of the Hölder norm. When $\beta = 1$, L_f is the Lipschitz constant of f (with respect to the manifold distance).

The Riemannian geometry also induces an intrinsic measure on \mathcal{M} . Let dV be the volume element on \mathcal{M} associated with the local Riemann volume form. Then (\mathcal{M}, dV) is a measure space. For any distribution $dP(x)$ on \mathcal{M} , it may have a density with respect to dV , that is, $dP(x) = p(x)dV(x)$, where p is the density function. In this paper, we consider densities that are Hölder continuous with respect to the metric $d_{\mathcal{M}}$ and square-integrable on (\mathcal{M}, dV) . Because $d_{\mathcal{M}}$ is intrinsic, the Hölder constants are intrinsically defined. Moreover, since the measure dV is intrinsic, dV -integrals such as the squared L^2 divergence $\int_{\mathcal{M}} (p(x) - q(x))^2 dV(x)$ between two distributions with densities p and q are also intrinsically defined.

2.4 Notations

Table 1 lists the default notations used in this paper. We may use abbreviated notation to omit the variable in an integral, e.g., $\int f dV = \int f(x) dV(x)$. The notation \wedge stands for the minimum of two numbers, i.e., $a \wedge b = \min\{a, b\}$. The paper considers the joint limiting process of sample size $n \rightarrow \infty$ and kernel bandwidth $\gamma \rightarrow 0$, but the main result is non-asymptotic and holds for finite sample size n which is sufficiently large.

With respect to a limiting process, e.g., $\gamma \rightarrow 0$, the default asymptotic notations are as follows: $f = O(|g|)$ means that there is constant C such that $|f| \leq C|g|$ eventually (meaning that there exists γ_0 s.t. when $\gamma < \gamma_0$ then $|g| \geq C|g|$). We use $O_x(\cdot)$ to denote big-O notation with the constant depending

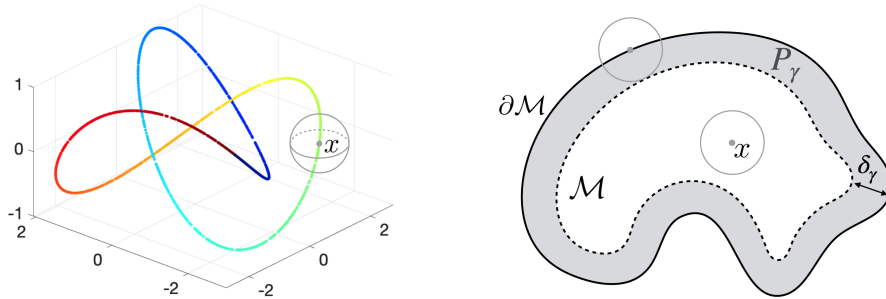


Figure 1: (Left) A one-dimensional manifold with no boundary (a closed curve) embedded in \mathbb{R}^3 , and an Euclidean ball centered at a point x on the manifold. (Right) Illustration of a two-dimensional manifold with boundary, showing the near-boundary set P_γ (gray belt), and two Euclidean balls centered at a point away from the boundary and another point on the boundary, respectively.

on object x . In this work, we consider constants that depend on the manifold \mathcal{M} and kernel function h as absolute ones and mainly focus on the constant dependence on data densities p and q . We will specify the constant dependence in the text, and we will also clarify the needed largeness of n or the smallness of γ for the bounds to hold. Additionally, $f \sim g$ means that $f, g \geq 0$ and there exist constants $C_1, C_2 > 0$ such that $C_1 g \leq f \leq C_2 g$ eventually; $f \gtrsim g$ means that $f \geq C_1 g$ eventually for some $C_1 > 0$; and $f \gg g$ means that for $f, g > 0$, $f/g \rightarrow \infty$ in the limit.

3 Theoretical properties of kernel tests on manifold data

In this section, we study the property of the kernel MMD-like statistic in (2) for manifold data. Note that the kernel statistic \hat{T} can be computed from any two datasets $\{x_i\}_{i=1}^{n_x}$ and $\{y_j\}_{j=1}^{n_y}$ as long as the bandwidth parameter γ is specified, and there is no need to estimate the intrinsic dimension d as an input parameter. The theory in this section studies the properties of the kernel test and the theoretical choice of γ when manifold structure is present in the high dimensional data. We begin by formulating the problem, introducing the local kernel, and stating the main result regarding the test size and power.

3.1 Manifold data in high-dimensional space

We state the necessary assumptions on the manifold data and sampling densities. An example of high dimensional image data satisfying our assumption is provided in Example 1, see Figure 2. In this section, we consider a compact manifold without a boundary:

Assumption 3.1 (Data manifold). \mathcal{M} is a d -dimensional compact connected C^∞ manifold isometrically embedded in \mathbb{R}^m without boundary.

An illustration of when $d = 1$ and $m = 3$ is shown in Figure 1(Left). Our theory extends when the manifold has a smooth boundary, which will be discussed in Section 4.1. This section assumes that the data densities p and q are supported on \mathcal{M} . In Section 4.2, we will discuss the extension of our analysis to the case where the data lie near the manifold and contain a certain type of additive Gaussian noise.

We introduce the following assumption on the Hölder regularity and boundedness of the data densities p and q . Recall the definition of $\mathcal{H}^\beta(\mathcal{M})$ in Section 2.3.

Assumption 3.2 (Data density). Data densities p and q are in $\mathcal{H}^\beta(\mathcal{M})$, $0 < \beta \leq 2$, and the Hölder constants of p and q are bounded by L_ρ , namely $L_\rho = \max\{L_p, L_q\}$. Since Hölder continuity implies

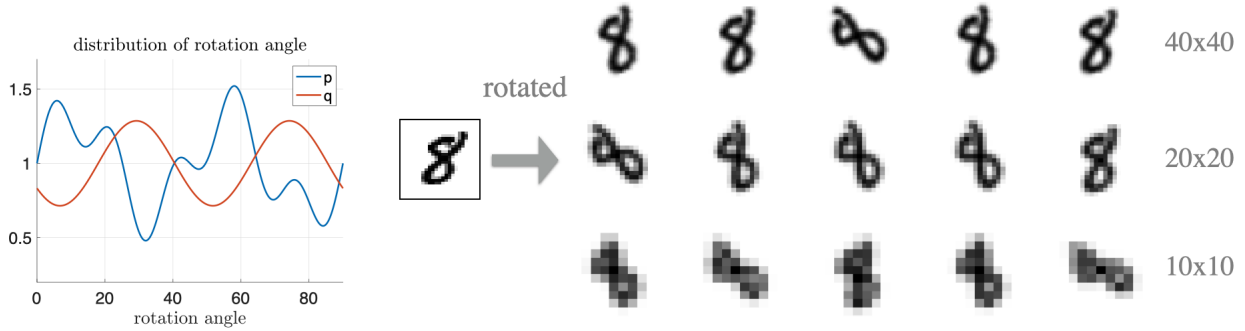


Figure 2: An example showing that the increase in the ambient dimension m does not affect the intrinsic dimensionality d nor the intrinsic geometry of the manifold data. An image of hand-written digit “8” is rotated by angles z and at different image sizes. The images for changing angle z lie on a one-dimensional manifold in the ambient space and approach a certain continuous limit as image resolution refines. The group element z has two distributions, which induce two distributions of data images in ambient space \mathbb{R}^m . When z changes from 0 to 2π the curve is closed and the data manifold has no boundary. When z changes from 0 to $\pi/2$ the curve has two endpoints and the data manifold has a boundary. The two-sample test results on this data are provided in Section 5.

continuity, due to compactness of \mathcal{M} , both densities are uniformly bounded, that is, there is constant ρ_{\max} such that

$$0 \leq p(x), q(x) \leq \rho_{\max}, \quad \forall x \in \mathcal{M}.$$

To illustrate that the manifold structure naturally arises in real-world data, we provide an example of high-dimensional data lying on intrinsically low-dimensional manifolds. In this example, the change in data densities q from p is induced by the change in densities on a latent manifold independent of the ambient space \mathbb{R}^m .

Example 1 (Manifold data with increasing m). Consider data samples in the form of images I_i that have $W \times W$ pixels and thus can be represented as vectors in \mathbb{R}^m , where $m = W^2$. The image I_i is generated by evaluating a continuous function on an image grid given a latent variable z_i . Specifically,

$$I_i(j_1, j_2) = F\left(\left(\frac{j_1}{W}, \frac{j_2}{W}\right); z_i\right), \quad 1 \leq j_1, j_2 \leq W,$$

where $F(u; z_i)$ is a smooth mapping from $u \in [0, 1] \times [0, 1]$ to \mathbb{R} that depends on a latent variable $z_i \in \mathcal{M}_z$. For instance, suppose \mathcal{M}_z is a d -dimensional rotation group $SO(2)$, and the mapping $F(\cdot; z)$ corresponds to applying the rotation action $z \in SO(2)$ to the image, as illustrated in Figure 2. Under generic assumptions on F , the continuous functions $F(\cdot; z)$ for all z lie on a d -dimensional manifold in the function space. This construction defines the embedding map ι from the manifold \mathcal{M}_z to $\mathbb{R}^{W \times W}$. In this example, when W increases, namely as the discretization gets finer, the image manifold in $\mathbb{R}^{W \times W}$ (up to a scalar normalization) also approaches a continuous limit determined by the latent manifold \mathcal{M}_z (the rotation angle) and the mapping F on $[0, 1]^2 \times \mathcal{M}_z$.

3.2 Local kernels on manifold and the population statistic

We consider local kernel $K_\gamma(x, y)$ defined as in (3) which is computed from Euclidean distances between data samples. In the term “local kernel”, “local” means a small kernel bandwidth parameter γ , and typically γ decreases as the sample size increases. The following class of non-negative differential kernel function h contains K_γ being the Gaussian RBF kernel as a special case.

Assumption 3.3 (Differentiable kernel). *We make the following assumptions about the function h , excluding the case where $h \equiv 0$:*

- (C1) *Regularity.* h is continuous on $[0, \infty)$, C^1 on $(0, \infty)$.
- (C2) *Decay condition.* h and h' are bounded on $(0, \infty)$ and have sub-exponential tail, specifically, $\exists a, a_k > 0$, s.t., $|h^{(k)}(\xi)| \leq a_k e^{-a\xi}$ for all $\xi > 0$, $k = 0, 1$. Without loss of generality, assume that $a_0 = 1$.
- (C3) *Non-negativity.* $h \geq 0$ on $[0, \infty)$.

Similar conditions on h have been used in [21] for kernelized graph Laplacian constructed from manifold data. For h that satisfies Assumption 3.3, we introduce the following moment constant of the kernel h ,

$$m_0[h] := \int_{\mathbb{R}^d} h(\|u\|^2) du, \quad (5)$$

which is finite due to (C2). By (C1),(C2) and that h is not a zero function, $m_0[h] > 0$. We note that $0 \leq K_\gamma(x, y) \leq 1$ for any x, y , where $K_\gamma(x, y)$ is induced by h as defined in (3), due to (C2) and (C3). Note that the kernel $K_\gamma(x, y)$ is not necessarily PSD, but the theory herein remains valid in this case. (For the prototypical choice of the Gaussian RBF kernel, the kernel is indeed PSD.) The non-negativity condition (C3) may be relaxed, as it is only used to guarantee that $m_0[h] > 0$ and in the extension to the manifold with boundary in Section 4.1. We assume (C3) for simplicity.

The following lemma establishes the approximation of a Hölder function f by its kernel integral on a manifold when γ is small; this result is necessary for our subsequent analysis.

Lemma 3.1 (Kernel integral on manifold). *Suppose \mathcal{M} satisfies Assumption 3.1, h satisfies Assumption 3.3, and f is in $\mathcal{H}^\beta(\mathcal{M})$, $0 < \beta \leq 2$, with Hölder constant L_f . Then there is $\gamma_0 > 0$ which depends on \mathcal{M} only, and constant C_1 that depends on (\mathcal{M}, h) , such that when $0 < \gamma < \min\{1, \gamma_0\}$, for any $x \in \mathcal{M}$,*

$$\left| \gamma^{-d} \int_{\mathcal{M}} h\left(\frac{\|x-y\|^2}{\gamma^2}\right) f(y) dV(y) - m_0[h] f(x) \right| \leq C_1 (L_f \gamma^\beta + \|f\|_\infty \gamma^2). \quad (6)$$

Specifically, γ_0 depends on manifold reach and curvature, and $C_1 > 0$ depends on manifold curvature and volume, the kernel function h (including the constants a, a_1 in Assumption 3.3(C2)), and the intrinsic dimensionality d .

In particular, if f is a constant function, then $L_f = 0$ and only the $O(\gamma^2)$ term remains in the bound in (6). The $O(\gamma^2)$ error is due to that the manifold has curvature while the local kernel function only accesses the Euclidean distance $\|x - y\|$ in the ambient space. When f is non-constant, the $O(\gamma^\beta)$ term results from the Taylor expansion (under manifold intrinsic coordinate) of f at x , and will be the leading term if $\beta < 2$. When $\beta = 2$, the bound in (6) becomes $O(\gamma^2)$, which echoes the $O(\gamma^2)$ error in Lemma 8 of [21] (the latter was proved for f with higher order regularity and under different technical assumptions). The constant γ_0 in Lemma 3.1 is for theoretical purposes, and, similar to other constant thresholds for the smallness of γ in later analysis, it is generally not to be computed in practice. We will clarify the choice of bandwidth γ in Remark 3.2. The proof of Lemma 3.1 follows the approach in [21] using standard techniques of differential geometry, and is included in Appendix A for completeness.

The empirical test statistic \widehat{T} is defined as in (2). Define the population kernel test statistic

$$\begin{aligned} T &:= \mathbb{E}_{x \sim p, y \sim p} K_\gamma(x, y) + \mathbb{E}_{x \sim q, y \sim q} K_\gamma(x, y) - 2\mathbb{E}_{x \sim p, y \sim q} K_\gamma(x, y) \\ &= \int_{\mathcal{M}} \int_{\mathcal{M}} K_\gamma(x, y) (p - q)(x)(p - q)(y) dV(x) dV(y), \end{aligned} \quad (7)$$

which equals the population (squared) kernel MMD when K_γ is PSD. Applying Lemma 3.1 gives the leading term in T as $\gamma \rightarrow 0$, as characterized in the following lemma. Define the squared L^2 -divergence between p and q as

$$\Delta_2 := \int_{\mathcal{M}} (p - q)^2 dV = \Delta_2(p, q). \quad (8)$$

Lemma 3.2. Under Assumptions 3.1, 3.2, 3.3, γ_0 and C_1 as in Lemma 3.1, when $0 < \gamma < \min\{1, \gamma_0\}$,

$$\gamma^{-d}T = m_0[h]\Delta_2 + r_T, \quad |r_T| \leq \tilde{C}_1(L_\rho + \rho_{\max})\gamma^\beta\Delta_2^{1/2}, \quad (9)$$

where $\tilde{C}_1 := 2C_1\text{Vol}(\mathcal{M})^{1/2}$ is a constant depending on (\mathcal{M}, h) .

We comment on the relationship between the population kernel statistic T and the L^2 -divergence Δ_2 between the two densities p and q . Recall that T by definition depends on the kernel bandwidth parameter γ . By definition, if $\Delta_2 = 0$, then $p = q$ in the L^2 sense and this implies that $T = 0$ for any $\gamma > 0$; If $\Delta_2 > 0$, then Lemma 3.2 gives that

$$\gamma^{-d}T = \Delta_2^{1/2} \left(m_0[h]\Delta_2^{1/2} + O(\gamma^\beta) \right),$$

which means that the right-hand side will be strictly positive when γ is sufficiently small, and as a result, T is also strictly positive (the magnitude is up to a scaling factor of γ^{-d}). When γ is not small enough, then it is possible that T becomes zero even $\Delta_2 > 0$.

3.3 Control of the deviation of \hat{T} from mean

We now control the deviation of the empirical test statistic \hat{T} around T , where the latter equals $\mathbb{E}\hat{T}$ up to an $O(1/n)$ bias. For the sample sizes of the two sets of samples, our analysis needs n_X and n_Y to grow proportionally to one another, namely, for some $\rho_X \in (0, 1)$,

$$n = n_X + n_Y, \quad n_X/n \rightarrow \rho_X, \quad \text{as } n_X, n_Y \rightarrow \infty. \quad (10)$$

As our analysis considers sufficiently large samples, we introduce the following technical condition based on (10) (the constant 0.9 can be changed to any positive number less than 1)

$$0.9\rho_X \leq \frac{n_X - 1}{n}, \quad 0.9(1 - \rho_X) \leq \frac{n_Y - 1}{n}, \quad 0 < \rho_X < 1. \quad (11)$$

The condition stands for the requirement of the largeness of n such that the balanced sizes of n_X and n_Y are achieved. We call (11) the *balancing condition* and assume it holds for all n . Since in our non-asymptotic result, we will derive the needed large n to guarantee the test level and power, the balancing condition (11) allows us to focus the characterization of the needed n on constants related to the manifold, the two densities, and the kernel, rather than the balancing of the two-sample sizes.

Proposition 3.4 proves a sample complexity result of the statistic \hat{T} , which controls the deviation $\hat{T} - T$ using the concentration of U-statistics. This estimation bound will be applied to control the upper tail of \hat{T} under H_0 and the lower tail of \hat{T} under H_1 respectively, and it can also be of independent interest. The U-statistic argument was used in [27, Theorem 10] but the deviation bound therein was based on the point-wise boundedness of the kernel and the influence of kernel bandwidth was not explicit. Here we apply a Bernstein-type argument which allows to reveal the role of the bandwidth. The proof adopts the classical decoupling technique of the U-statistics [32] and is included in Appendix A for completeness.

Proposition 3.4 (Control of $|\hat{T} - T|$). Under Assumption 3.1, 3.2, 3.3, and the balancing condition (11). Define

$$c := 0.9 \min\{\rho_X, 1 - \rho_X\}, \quad \nu := (m_0[h^2] + 1)\rho_{\max}. \quad (12)$$

Then, there is a constant $C_1^{(2)} > 0$ depending on (\mathcal{M}, h) such that when $0 < \gamma < \min\{1, \gamma_0, (C_1^{(2)})^{-1/2}\}$, for any $0 < \lambda < 3\sqrt{c\nu\gamma^d n}$, with probability $\geq 1 - 3e^{-\lambda^2/8}$,

$$\hat{T} \leq T + \frac{2}{cn} + 4\lambda\sqrt{\frac{\nu\gamma^d}{c n}},$$

and with probability $\geq 1 - 3e^{-\lambda^2/8}$,

$$\widehat{T} \geq T - \frac{2}{cn} - 4\lambda \sqrt{\frac{\nu \gamma^d}{c n}}.$$

The constant $C_1^{(2)}$ corresponds to the constant C_1 in Lemma 3.1 with the function h replaced by h^2 .

Due to the fact that the proof of Proposition 3.4 reduces the concentration of the U-statistic to that of an $O(n)$ -term independent sum, which is the same as the linear-time statistic (see Remark 3.4), an $O(n^{-1/2})$ fluctuation of the statistics \widehat{T} around the mean is obtained (without considering γ in the big-O notation and up to the $O(n^{-1})$ bias). It is worth noting that, under H_0 , the deviation is expected to scale as $O(n^{-1})$ [27, 16]. In Section 6, we will discuss the possible influence on the asymptotic rate for detecting $q \neq p$. In practice, the testing threshold is usually estimated empirically using bootstrap methods rather than chosen according to theory, because the theoretical thresholds obtained by inequality can be over-conservative and those by approximation can be less accurate. See Section 5 for more details about the algorithm in practice.

3.4 Test level and power

We are ready to derive the main theorem which characterizes the kernel test's level and power when applied to manifold data at a finite sample size.

Theorem 3.5 (Power of kernel test). *Under Assumptions 3.1, 3.2, 3.3, and the balancing condition (11), let the constants γ_0 be as in Lemma 3.1, \tilde{C}_1 be as in Lemma 3.2, and c, ν , and $C_1^{(2)}$ be as in Proposition 3.4. Define $\lambda_1 := \sqrt{8 \log(3/\alpha_{\text{level}})}$, and let the threshold for the test be $t_{\text{thres}} := 2/(cn) + 4\lambda_1 \sqrt{\nu \gamma^d / (cn)}$. For $q \neq p$ under H_1 , suppose $\Delta_2 = \int_{\mathcal{M}} (p - q)^2 dV > 0$. Then, when γ is small enough such that $0 < \gamma < \min \left\{ 1, \gamma_0, (C_1^{(2)})^{-1/2} \right\}$ and*

$$\tilde{C}_1 (L_\rho + \rho_{\max}) \gamma^\beta < 0.1 m_0 [h] \Delta_2^{1/2}, \quad (13)$$

and meanwhile, for some constant $\lambda_2 > 0$, n is large enough such that

$$\gamma^d n > \max \left\{ \frac{1}{c\nu} \left(\frac{\max\{\lambda_1, \lambda_2\}}{3} \right)^2, \frac{10}{cm_0[h]\Delta_2}, \frac{\nu}{c} \left(\frac{8(\lambda_1 + \lambda_2)}{m_0[h]\Delta_2} \right)^2 \right\}, \quad (14)$$

then

$$\mathbb{P}[\widehat{T} > t_{\text{thres}} | H_0] \leq \alpha_{\text{level}}, \quad \mathbb{P}[\widehat{T} \leq t_{\text{thres}} | H_1] \leq 3e^{-\lambda_2^2/8}. \quad (15)$$

We give a few comments to interpret the result in Theorem 3.5. First, the choice of the test threshold in the theorem is a theoretical one to facilitate our analysis, especially to obtain the dependence of test power on various factors like the dimensionality of data. Second, Theorem 3.5 considers a fixed alternative q , and the bound of testing power holds for finite samples and finite γ . To obtain a test power close to 1, namely a Type-II error in (15) as small as ϵ , one can make $\lambda_2 = \sqrt{8 \log(3/\epsilon)}$, and then the theorem guarantees the test power when γ can be chosen to satisfy (13) and (14) simultaneously, which requires n to be large enough given Δ_2 . This also leads to an argument for, with large n , what is the smallest Δ_2 (scales with a negative power of n) such that the H_1 can be correctly rejected using the kernel tests (with probability at least $1 - \epsilon$). We call this the ‘‘rate-for-detection’’ and it is derived in Corollary 3.6. At last, in Theorem 3.5, only the intrinsic dimensionality d affects the testing power but not the ambient space dimensionality m . The constants Δ_2 , ρ_{\max} , and L_ρ are determined by p and q as Hölder functions on (\mathcal{M}, dV) and are intrinsically defined.

Remark 3.1 (Constant m_0). The constants $m_0[h^2]$ (appearing in the definition of ν) and $m_0[h]$ are integrals of the kernel function in \mathbb{R}^d defined as in (5). The explicit values for the Gaussian RBF kernel are as follows:

Example 2 (Constants for Gaussian h). When $h(r) = e^{-r/2}$,

$$m_0[h] = \int_{\mathbb{R}^d} e^{-|u|^2/2} du = (2\pi)^{d/2}, \quad m_0[h^2] = \int_{\mathbb{R}^d} e^{-|u|^2} du = \pi^{d/2}.$$

For general h , both constants depend on d .

We consider the scenario where $\Delta_2(p, q)$ is allowed to decrease to zero as the sample size increases. The following corollary shows that the kernel test can achieve a positive test power (at the test level) as long as $\Delta_2 \gtrsim n^{-2\beta/(d+4\beta)}$, and is asymptotically consistent (power approaches 1) when Δ_2 is greater than that order.

Corollary 3.6 (Rate-for-detection). *Under the same assumptions as in Theorem 3.5, suppose as n increases, $\gamma \sim n^{-1/(d+4\beta)}$, the densities p and q satisfy that their squared L^2 -divergence Δ_2 is positive and is less than an $O(1)$ constant determined by ρ_{\max} , d and h , and, for $0 < \epsilon < 1$, with large n ,*

$$\Delta_2 > c_3 \left(\log \frac{1}{\alpha_{\text{level}}} + \log \frac{1}{\epsilon} \right)^{1/2} n^{-2\beta/(d+4\beta)}, \quad (16)$$

where the constant c_3 depends on constants $\{L_\rho, \rho_{\max}, \rho_X, d, \beta\}$ and (\mathcal{M}, h) and $\alpha_{\text{level}} < 1/2$. Then, for large enough n , the kernel test achieves a test level α_{level} and a test power at least $1 - \epsilon$. In particular, the test power $\rightarrow 1$ as $n \rightarrow \infty$ if $\Delta_2 \gg n^{-2\beta/(d+4\beta)}$.

Remark 3.2 (Choice of bandwidth). As shown in Corollary 3.6, when Δ_2 is small as in the regime therein, the bandwidth needs to scale with $n^{-1/(d+4\beta)}$ so that the test can have power. Such a kernel bandwidth $\gamma \rightarrow 0$ as n increases. The analysis suggests using small-bandwidth kernels for the test to detect small changes in distribution when large data samples are available. In contrast, the median distance choice of bandwidth [27] may lead to γ of order $O(1)$ in this case: on a manifold of diameter $O(1)$, suppose the data density is uniform, then the median of pairwise distance is generally $O(1)$. Thus the median distance γ may not be optimal for high-dimensional data, for example, when data lie on or near intrinsically low-dimensional manifolds or sub-manifolds, and there are sufficiently many samples in the dataset to detect a small departure of the density. We show in Section 5 that high-dimensional data kernel tests with a smaller bandwidth can outperform those with the median distance bandwidth in experiments. Theoretically, note that for kernel tests on data in Euclidean space, the optimal γ is shown to also scale with a negative power n to achieve minimax rate of detection [40]. We further discuss the rate and the relation to this work in the discussion section.

In practice, kernel bandwidth is a hyper-parameter that can be determined by some cross-validation procedure at the cost of additional computation. The optimal choice of bandwidth depends on data distribution and sample size and would be difficult to predict theoretically. In particular, our theory (starting from Lemma 3.1 to Theorem 3.5) needs γ to be less than some $O(1)$ constant, and these theoretical constants can be difficult to obtain in practice especially when the data manifold is unknown. Our analysis does not suggest estimating these constants as a manner to gauge whether the kernel bandwidth is proper or not. Instead, the interpretation of our theory should be that, under the necessary conditions, there exists a γ such that the kernel test is guaranteed to distinguish the density departure. Such γ can be found, e.g., by cross-validation in practice. Of course, this only happens with sufficient data samples, and when the sample size is not large enough then the test power cannot be guaranteed - the selected γ in practice may still lead to a test with power that is not guaranteed by our theory here. Our rate for detection result provides a theoretical scaling of γ , which may provide guidance for the range of the value to search for in practice. For example, if the manifold intrinsic dimension is known *a priori* or can be estimated from data

[46, 25, 38, 9, 44], our theoretical scaling would suggest how the bandwidth parameter should scale as the sample size increases. Generally, when more data samples are available, the theory suggests searching the smaller value range from the median distance, which can improve the detection ability of the kernel test for small density departures.

Remark 3.3 (Higher Hölder regularity). As shown in the proof of Corollary 3.6, the improvement of detection rate from higher regularity β is via analyzing how to fulfill (13) by setting γ sufficiently small. The condition (13) is based on the bound of $|r_T|$ in Lemma 3.2, and the latter is proved by Lemma 3.1 which gives an $O(\gamma^{\beta \wedge 2})$ bound in (6). This means that when $\beta > 2$ (and $\|p - q\|_\infty > 0$) the bound of $|r_T|$ will remain $O(\gamma^2)$. As a result, higher Hölder regularity of the densities beyond two will not further improve the rate under the current analysis.

Remark 3.4 (Linear-time statistic). When $n_X = n_Y = 2m$, the linear-time test statistic, following [27, Section 6], is defined as $\widehat{T}_{\text{lin}} = \frac{1}{m} \sum_{i=1}^m h(z_{2i-1}, z_{2i})$, where $z_i = (x_i, y_i)$ and $h(z_i, z_j) := K_\gamma(x_i, x_j) - K_\gamma(x_i, y_j) - K_\gamma(y_i, x_j) + K_\gamma(y_i, y_j)$. The construction in [27] is for kernel MMD test, but \widehat{T}_{lin} is well-defined when the kernel K_γ is not PSD. The statistic \widehat{T}_{lin} can be computed using $O(n)$ time and memory. The mean $\mathbb{E}\widehat{T}_{\text{lin}} = T$ as has been analyzed in Lemma 3.2; The deviation of \widehat{T}_{lin} from mean observes bounds of the same order as in Proposition 3.4, since the finite-sample concentration of \widehat{T}_{lin} is that of an independent sum of $n_X/2$ terms (technically the decoupling argument in the proof of Proposition 3.4 reduces the concentration of the U-statistic to that of the $(2i - 1, 2i)$ -indexed independent sum). As a result, the same test power analysis and rate of detection as proved in Theorem 3.5 and Corollary 3.6 hold for the linear-time statistic \widehat{T}_{lin} .

4 Theoretical extensions to manifold with boundary and noisy data

In this section, we extend the analysis in Section 3 to two important cases, namely when the data manifold has a boundary and data has additive noise in high dimensional ambient space.

4.1 Manifold with boundary

In many scenarios the data manifold has a boundary. For instance, when the range of rotation angle in Example 1 is less than $[0, 2\pi]$ the curve in the image space is not closed, and this is an example of manifold having boundaries, also see Figure 2. Another reason to consider boundary is the applicability of our theory to the Euclidean case (the manifold is “flat”), where after assuming compact support of the distributions the support domain will have a boundary, see more in Remark 4.1.

For our analysis, when a data point x approaches the manifold boundary the support of the local kernel will also intersect with the boundary, which makes the expression of local kernel integral in Lemma 3.1 not hold and voids the subsequent analysis. The current section is devoted to extending the theory in Section 3 to the case of the manifold with boundary by first extending Lemma 3.1. We assume

Assumption 4.1. \mathcal{M} is a d -dimensional compact C^∞ sub-manifold isometrically embedded in \mathbb{R}^m , where the boundary $\partial\mathcal{M}$ is also C^∞ .

The analysis proceeds using similar techniques and is based on the local kernel integral lemma (Lemma 4.1), which handles when x is on or near to $\partial\mathcal{M}$. Theorem 3.5 then extends under an additional Assumption 4.2 and certain modifications of the constants and condition (13), see the specifics in Theorem 4.3.

Remark 4.1 (Euclidean space). When data densities p and q are compactly supported on some domain Ω in \mathbb{R}^m and Ω has a smooth boundary, this is a special case of the manifold-with-boundary setting where $d = m$. Our theoretical result thus covers such cases. When m is large, there is a curse-of-dimensionality revealed by the γ^d factor in the required lower bound of n in the condition (14).

We start by establishing the following lemma, which is the counterpart of Lemma 3.1.

Lemma 4.1. *Suppose \mathcal{M} satisfies Assumption 4.1, h satisfies Assumption 3.3, and f is in $\mathcal{H}^\beta(\mathcal{M})$, $0 < \beta \leq 2$, with Hölder constant L_f . Let $d_E(x, \partial\mathcal{M}) := \inf_{y \in \partial\mathcal{M}} \|x - y\|$, and define $\delta_\gamma := \sqrt{\frac{d+10}{a} \gamma^2 \log \frac{1}{\gamma}}$. Then, there is $\gamma'_0 > 0$ which depends on \mathcal{M} only, such that when $0 < \gamma < \min\{\gamma'_0, 1\}$,*

- (i) *For any $x \in \mathcal{M}$ such that $d_E(x, \partial\mathcal{M}) > \delta_\gamma$, (6) holds.*
- (ii) *There is constant C'_1 that depends on (\mathcal{M}, h) , such that for any x s.t. $d_E(x, \partial\mathcal{M}) \leq \delta_\gamma$, there exists a function $m_0^{(\gamma)}[h](x)$ depending on γ s.t. $0 \leq m_0^{(\gamma)}[h](x) \leq m_0[h]$ for all x and*

$$\left| \gamma^{-d} \int_{\mathcal{M}} h \left(\frac{\|x - y\|^2}{\gamma^2} \right) f(y) dV(y) - m_0^{(\gamma)}[h](x) f(x) \right| \leq C'_1 (L_f \gamma^{\beta \wedge 1} + \|f\|_\infty \gamma^2). \quad (17)$$

Similarly, as in Lemma 3.1, γ'_0 depends on manifold reach and curvature, and the constant C'_1 depends on manifold curvature and volume, and the kernel function h . The lemma shows that the error bound at x that is δ_γ away from \mathcal{M} is $O(\gamma^{\beta \wedge 2})$ same as before, and at x that is within δ_γ distance from \mathcal{M} is $O(\gamma^{\beta \wedge 1})$. This reflects the degeneracy of the kernel integral approximation at x , which is close to the manifold boundary.

When $\gamma < \min\{\gamma'_0, 1\}$, we define $P_\gamma := \{x \in \mathcal{M}, d_E(x, \partial\mathcal{M}) \leq \delta_\gamma\}$, which is the δ_γ -near-boundary set as shown in Figure 1(Right). To extend Lemma 3.2, we introduce the assumption that the major part of Δ_2 is not coming from the integral on P_γ .

Assumption 4.2. *For $q \neq p$, there are positive constants γ''_0 and C_3 possibly depending on \mathcal{M} (and independent from p and q), such that when $\gamma < \gamma''_0$,*

$$\int_{P_\gamma} (p - q)^2 dV \leq C_3 \delta_\gamma \int_{\mathcal{M}} (p - q)^2 dV.$$

We then extend Lemma 3.2 which bounds the error between $\gamma^{-d}T$ and $m_0[h]\Delta_2(p, q)$ in the following lemma.

Lemma 4.2. *Under Assumptions 3.2, 3.3, 4.1, 4.2, γ'_0 as in Lemma 4.1. Then, when $0 < \gamma < \min\{1, \gamma'_0, \gamma''_0\}$, we have that*

$$\gamma^{-d}T = m_0[h]\Delta_2 + r_T, \quad |r_T| \leq C_3 \delta_\gamma m_0[h]\Delta_2 + (L_\rho + \rho_{\max})(\tilde{C}_1 \gamma^\beta + \tilde{C}'_2 \gamma^{\beta \wedge 1} \delta_\gamma) \Delta_2^{1/2}, \quad (18)$$

where the constants \tilde{C}_1 (as in Lemma 3.2) and \tilde{C}'_2 depend on (\mathcal{M}, h) only, including manifold curvature and volume, the regularity and volume of $\partial\mathcal{M}$, and the intrinsic dimensionality d .

Next, we extend Proposition 3.4 after replacing the constant $C_1^{(2)}$ with some $C_1'^{(2)}$, and γ_0 with γ'_0 , in the statement (details in the proof), and this allows extending Theorem 3.5 to a data manifold with smooth boundary in the following theorem.

Theorem 4.3. *Under Assumptions 3.2, 3.3, 4.1, and 4.2, the same bound of test power as in Theorem 3.5 holds with the following changes: (i) replacing the constant $C_1^{(2)}$ with $C_1'^{(2)}$ and requiring $0 < \gamma < \min\{1, \gamma'_0, \gamma''_0\}$, (ii) condition (13) is replaced by*

$$C_3 \delta_\gamma < 0.05, \quad (L_\rho + \rho_{\max}) \left(\tilde{C}_1 \gamma^\beta + \tilde{C}'_2 \gamma^{\beta \wedge 1} \delta_\gamma \right) < 0.05 m_0[h] \Delta_2^{1/2}, \quad (19)$$

where the constants \tilde{C}_1 and \tilde{C}'_2 are as in Lemma 4.2 and depend on (\mathcal{M}, h) only.

Based on (19), which is again implied by the technical bound in (18), the above theorem induces a detection rate similar to in Corollary 3.6: Specifically, first note that $\delta_\gamma \sim \gamma\sqrt{\log(1/\gamma)}$ which is $o(1)$ as $\gamma \rightarrow 0$, thus $C_3\delta_\gamma < 0.05$ is satisfied when γ is less than some $O(1)$ threshold. In the second equation in (19), note that $\gamma^{\beta\wedge 1}\delta_\gamma \sim \gamma^{\beta\wedge 1+1}\sqrt{\log(1/\gamma)}$ which is dominated by γ^β (when $\beta = 2$, there is a factor of $\sqrt{\log(1/\gamma)}$). Thus the smallness of γ requirement is the same as in the proof of Corollary 3.6 (up to a factor of $\sqrt{\log(1/\gamma)}$). The largeness of n requirement is the same as before. As a result, the rate of detection for small enough Δ_2 in the order of n and the optimal scaling of γ are the same as in Corollary 3.6.

In case when Assumption 4.2 does not hold, one can derive upper bound of $|r_T|$ using similar techniques as in Lemma 4.2, and the rest of the analysis also generalizes. As the bound of $|r_T|$ will be worsen (due to that the kernel integral approximation error degenerates near the boundary as shown in Lemma 4.1(ii)), the resulting rate is also worse than in Theorem 4.3. Details are omitted.

In line with the theoretical results, the experiments in Section 5 are conducted on manifold data where \mathcal{M} has a boundary. In Section 5.1, the data manifold is a continuous curve in the ambient space with endpoints. In Section 5.2, the original MNIST image data lie close to a collection of sub-manifolds in the ambient space, and it is also a case of a manifold with a boundary.

4.2 Near-manifold noisy data

In applications, data points may not lie exactly on the low-dimensional manifold but only near it. Since kernel $K_\gamma(x, y)$ is computed from Euclidean distances among data points, one can expect that if data samples are lying within a distance proportional to γ from the manifold \mathcal{M} , then the integration of kernel $K_\gamma(x, y)$ over such data distributions will preserve the magnitude to be of order γ^d and will not have a curse of dimensionality.

An important case is when near-manifold data are produced by adding Gaussian noise, which is distributed as $\mathcal{N}(0, \sigma^2 I_m)$, to data points that are lying on a manifold. In this case, to make the off-manifold perturbation to be of length up to constant times of γ (with high probability), it allows σ to be up to $c\gamma/\sqrt{m}$ for some $c > 0$. Here, we show that Theorem 3.5 can be extended under this noise regime for Gaussian kernel h . The analysis may also extend to other types of kernel functions.

Specifically, let $x_i = x_i^{(c)} + \xi_i^{(1)}$, $x_i^{(c)} \sim p_{\mathcal{M}}$, $\xi_i^{(1)} \sim \mathcal{N}(0, \sigma_{(1)}^2 I_m)$, and $y_i = y_i^{(c)} + \xi_i^{(2)}$, $y_i^{(c)} \sim q_{\mathcal{M}}$, $\xi_i^{(2)} \sim \mathcal{N}(0, \sigma_{(2)}^2 I_m)$, where the manifold clean data $x_i^{(c)}$ and $y_i^{(c)}$ are independent from the ambient space Gaussian noise $\xi_i^{(1)}$ and $\xi_i^{(2)}$. When $p_{\mathcal{M}}$ and $q_{\mathcal{M}}$ satisfies Assumption 3.2 and h is Gaussian kernel, Theorem 3.5 extends when, for some $c > 0$,

$$\sigma_{(1)}^2 + \sigma_{(2)}^2 \leq \frac{c^2}{m}\gamma^2. \quad (20)$$

The argument is based on that the proof of Theorem 3.5 relies on the approximation of kernel integrals $\mathbb{E}_{x \sim p, y \sim p} K_\gamma(x, y)$ and the boundedness of $\mathbb{E}_{x \sim p, y \sim p} K_\gamma(x, y)^2$ at the order $O(\gamma^d)$, and similarly with $\mathbb{E}_{x \sim p, y \sim q}$, $\mathbb{E}_{x \sim q, y \sim q}$. Thus, when kernel h is Gaussian, and p (and q) equals $p_{\mathcal{M}}$ (and $q_{\mathcal{M}}$) convolved with a Gaussian with coordinate variance $\lesssim \gamma^2/m$ in \mathbb{R}^m , these integrals can be shown to be equivalent to those integrated over $p_{\mathcal{M}}$ and $q_{\mathcal{M}}$ with another Gaussian kernel having bandwidth $\tilde{\gamma}$, where $\tilde{\gamma}/\gamma$ is bounded between 1 and the absolute constant $\sqrt{1 + c^2/m}$. As a result, the integrals of $K_\gamma(x, y)$ and $K_\gamma(x, y)^2$ can be computed same as before in Lemma 3.2 and Proposition 3.4, leading to a result of Theorem 3.5 after replacing the roles of p and q with $p_{\mathcal{M}}$ and $q_{\mathcal{M}}$. Details are left to Appendix A.3.

This suggests that when the coordinate-wise noise level σ in \mathbb{R}^m is bounded at the level of γ/\sqrt{m} , the behavior of the two-sample test with kernel $K_\gamma(x, y)$ applied to manifold-plus-noise data is essentially close to as if applied to the clean on-manifold data, and the testing power is determined by the on-manifold distributions $p_{\mathcal{M}}$ and $q_{\mathcal{M}}$. Experiments of data with additive Gaussian noise are given in Section 5, which verifies this theoretical prediction. In practice, we observe that the testing performances on clean and

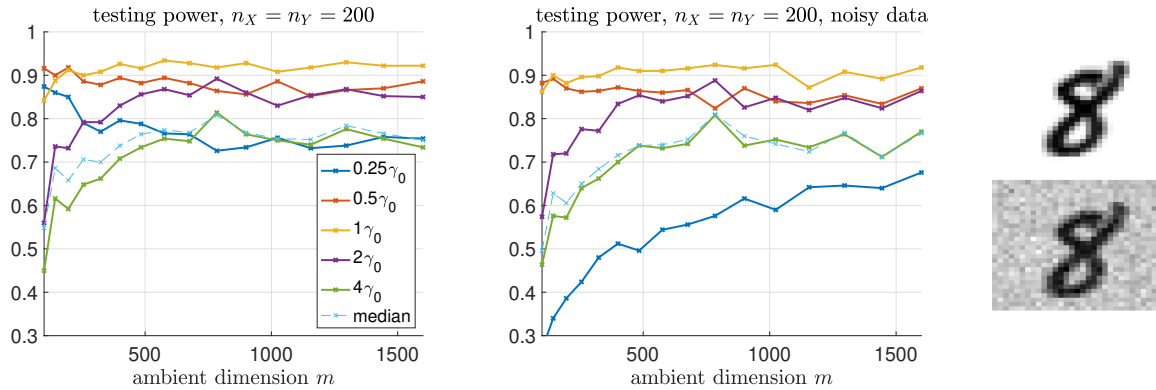


Figure 3: An example of simulated manifold data on which the kernel test power does not drop as the ambient dimension m increases, where the intrinsic dimension d remains constant. Gaussian kernel test statistics are computed on two datasets of rotated images with different distributions of rotation angles. Images are of sizes $10 \times 10, \dots, 40 \times 40$, and thus m increases from 100 to 1600. The test is computed with 5 values of kernel bandwidth as in (21), and that is chosen by the median distance from the data. The test power is estimated using $n_{\text{run}} = 500$. (Left) Results on clean images. (Middle) Results on images with additive Gaussian noise, where the noise level is chosen to be small and satisfies the condition in Section 4.2. (Right) Example clean and noisy images (size 30×30).

noisy data will stay close for small noise level σ , and start to show discrepancies when σ exceeds a certain level.

5 Numerical experiments

In this section, we present several numerical examples to demonstrate the validity of our theory. We first study a synthetic example of image data lying on a manifold, and then a density departure example using the MNIST dataset. The summary of the algorithm, including computation of the test threshold by bootstrap [1], is provided in Appendix B. Code available at the public repository https://github.com/yxcheng/manifold_mmd.

The notations are as follows: n_{run} is the number of replicas used to estimate the test power, and n_{boot} the number of bootstrap samples in computing the test threshold. We set the test level $\alpha_{\text{level}} = 0.05$ throughout. In our experiments, we test over a range of kernel bandwidth parameters γ . In practice, γ can also be chosen adaptively from data, e.g., the *median distance bandwidth* is set to be the median of all pairwise distances in the two sample datasets. Our theory in Section 3 suggests that the median distance γ may not always be the optimal choice: for manifold data of intrinsically low dimensionality, kernels with smaller bandwidth can achieve better testing power when there are sufficiently many samples. We verify this in experiments. In addition, we examine the Gaussian kernel and several possibly non-PSD kernels, and verify that the latter can also achieve high test power as suggested by our theory.

5.1 Images with differently distributed rotation angles

5.1.1 Clean data

We construct two datasets consisting of randomly rotated copies of an image of the handwritten digit ‘8’, which are resized to be of different resolutions. The data-generating process was introduced in Example 1 and illustrated in Figure 2. This experiment is designed such that we specify the true distributions on the latent manifold (rotation angles), which induces the distributions of observed manifold data. The distributions p and q of the two datasets are induced by different rotation angle distributions, and the

densities of rotation angles (between 0 to 90 degrees) are shown in the left of Figure 2. The image size changes from 10×10 to 40×40 , and as a result, the data dimensionality increases from 100 to 1600. Note that since the rotation is only up to $\pi/2$, the corresponding manifold is a 1D curve with two endpoints, namely a manifold with a boundary.

Note that the image pixel values maintain the same magnitude as W increases, and then the value of $\frac{1}{m} \sum_{u=1}^m I_i(u)^2$ approaches an $O(1)$ limit, which is the squared integral of the underlying continuous function on $[0, 1]^2$. This means that the image data vectors of size $W \times W$ need to divide by \sqrt{m} , $m = W^2$, so as to obtain isometric embedding of a manifold of diameter $O(1)$ in \mathbb{R}^m . In experiments we use bandwidth γ to resized images, can we call γ/\sqrt{m} the “pixel-wise bandwidth”. The pixel-wise bandwidth corresponds to the “ γ ” in theory in Section 3.

In computing the Gaussian kernel test statistics, we use bandwidth parameters over 5 values such that

$$\frac{\gamma}{\sqrt{m}} = \gamma_0 \left\{ \frac{1}{4}, \frac{1}{2}, 1, 2, 4 \right\}, \quad m = W^2, \quad W = 10, \dots, 40, \quad (21)$$

with $\gamma_0 = 20$, which we call the “baseline pixel-wise bandwidth”. The median distance gives the pixel-wise bandwidth is about 70. Since the grayscale images take pixel values between 0 and 255, the pixel-wise bandwidth being 20 is relatively small, and is smaller than that chosen by the median distance. The estimated two-sample testing power on clean images is shown in Figure 3 (Left), which is computed using $n_{\text{boot}} = 400$ and $n_{\text{run}} = 500$. It can be seen that all the bandwidth choices give certain test power, which is consistent across m as m increases (showing a tendency of convergence after m exceeds 500 till 1600). The performance with pixel-wise bandwidth equal to 20 appears to be the best and is better than the bandwidth by median distance.

5.1.2 Noisy data

We add pixel-wise Gaussian noise of standard deviation $\sigma_0 = 20$ to the resized image data of dimension m , that is, $\sigma_0 = \gamma_0$ the baseline pixel-wise bandwidth in the previous clean data experiment. This falls under the scenario in Section 4.2: As was pointed out in the experiment with clean data, normalized clean image I_i/\sqrt{m} lie on an $O(1)$ manifold, where I_i has size $W \times W$, $m = W^2$, and thus the pixel-wise bandwidth corresponds to the “ γ ” in the theory. If we add Gaussian noise $\mathcal{N}(0, \sigma_0^2 I_m)$ to the clean image I_i , it corresponds to adding noise $\mathcal{N}(0, (\sigma_0^2/m) I_m)$ to I_i/\sqrt{m} . Thus σ_0/\sqrt{m} is the “ σ ” in Section 4.2. The small noise regime in Section 4.2 requires “ $\sigma < c\gamma/\sqrt{m}$ ” for some constant c , and here, “ γ ” there is γ_0 , and “ σ ” there is σ_0/\sqrt{m} , thus the condition translates into $\sigma_0/\sqrt{m} < c\gamma_0/\sqrt{m}$, which is satisfied if we set $\sigma_0 = \gamma_0$.

An example pair of clean and noise-corrupted images are shown in Figure 3 (Right). We conduct the two-sample testing experiments in the same way as in the experiment with clean data, and the the estimated testing power is shown in Figure 3 (Middle). The performance with the four pixel-wise bandwidth, which is greater than $\gamma_0/2$ are about the same as on the clean data; With the smallest pixel bandwidth $\gamma_0/4$, the test power degenerates and becomes worse than the choice by median distance, and the drop is more significant when dimensionality m is small. This suggests that this kernel bandwidth is too small for the amount of additive noise at the values of m and sample size n_X and n_Y .

5.2 Density departure in MNIST dataset

In this experiment, we compute the Gaussian kernel two-sample test on the original MNIST digit image dataset, where samples are of dimensionality 28×28 . The data densities p and q are generated in the following way: p is uniformly subsample from the MNIST dataset, namely $p = p_{\text{data}}$. Though we only have finite samples (the MNIST dataset has 70000 images in 10 classes) of p_{data} , as we subsample $n_X = 6000$ from the whole dataset, it is approximate as if drawn from the population density p . q is constructed as a mixture of $q = 0.975p_{\text{data}} + 0.025p_{\text{cohort}}$, where p_{cohort} is the distribution of a local cohort within the

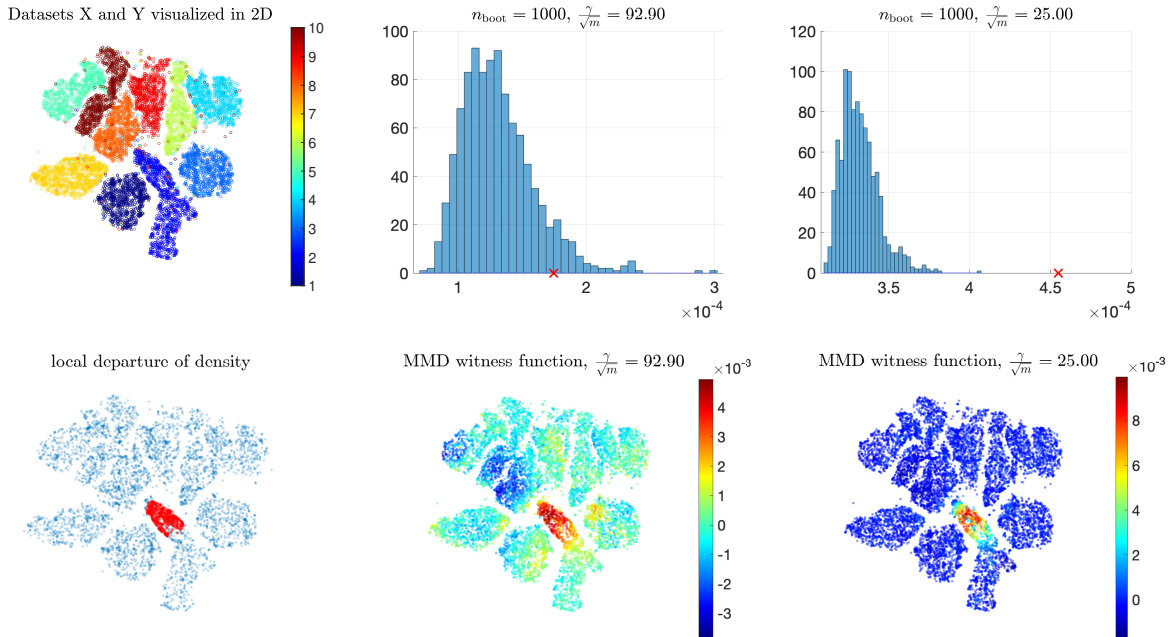


Figure 4: Kernel two-sample test to detect a local density departure of the MNIST image data distributions. (Top left) Datasets X and Y are visualized in 2D by tSNE, colored by 10-digit class labels. (Top middle and right) Kernel test statistic \hat{T} (red cross) plotted against the histogram of test statistic under H_0 computed by bootstrap [1] (blue bar, see more in Appendix B. The middle plot is for the Gaussian kernel test using median distance γ , and the right plot is by using a smaller γ . (Bottom left) The local cohort density p_{cohort} is illustrated by red dots. (Bottom middle and right) The witness function defined in (22) for kernel using median distance γ and a smaller bandwidth, respectively.

samples of digit “1”, having about 1700 samples. Since n_Y is set to be about 6000, and we subsample about 150 from the local cohort, the way we simulate samples in Y is approximately as if drawn from the density q . The local cohort corresponding to p_{cohort} is illustrated in Figure 4 (Bottom left), indicating the place where the density q departs from p . The experiment is conducted on one realization of dataset X and Y , where $n_X = 6000$, $n_Y = 5990$.

We apply the kernel test with two bandwidths, one using the median distance, which gives the pixel-wise bandwidth $\gamma/\sqrt{m} = 92.9$, and here $m = 28^2$; and the other takes $\gamma/\sqrt{m} = 25$. The test statistic \hat{T} under H_1 vs. the histogram under H_0 computed by bootstrap with $n_{\text{boot}} = 1000$ are shown in the top panel of Figure 4. It can be seen that with the smaller bandwidth, the test statistic shows a more clear rejection of H_0 , indicating better testing power.

The *witness function* of kernel MMD [27] is defined as

$$\hat{w}(x) = -\frac{1}{n_X} \sum_{i=1}^{n_X} K_\gamma(x, x_i) + \frac{1}{n_Y} \sum_{j=1}^{n_Y} K_\gamma(x, y_j), \quad (22)$$

and we visualize \hat{w} with the Gaussian kernel as heat-map on the 2D embedding in the bottom panel of Figure 4. The witness function indicates where the two densities differ. Compared with the ground truth in the bottom left plot of the departure p_{cohort} , the witness function computed with the local kernel better detects the density departure than the median distance kernel, and this is consistent with the better test statistic separation in the top panel plots.

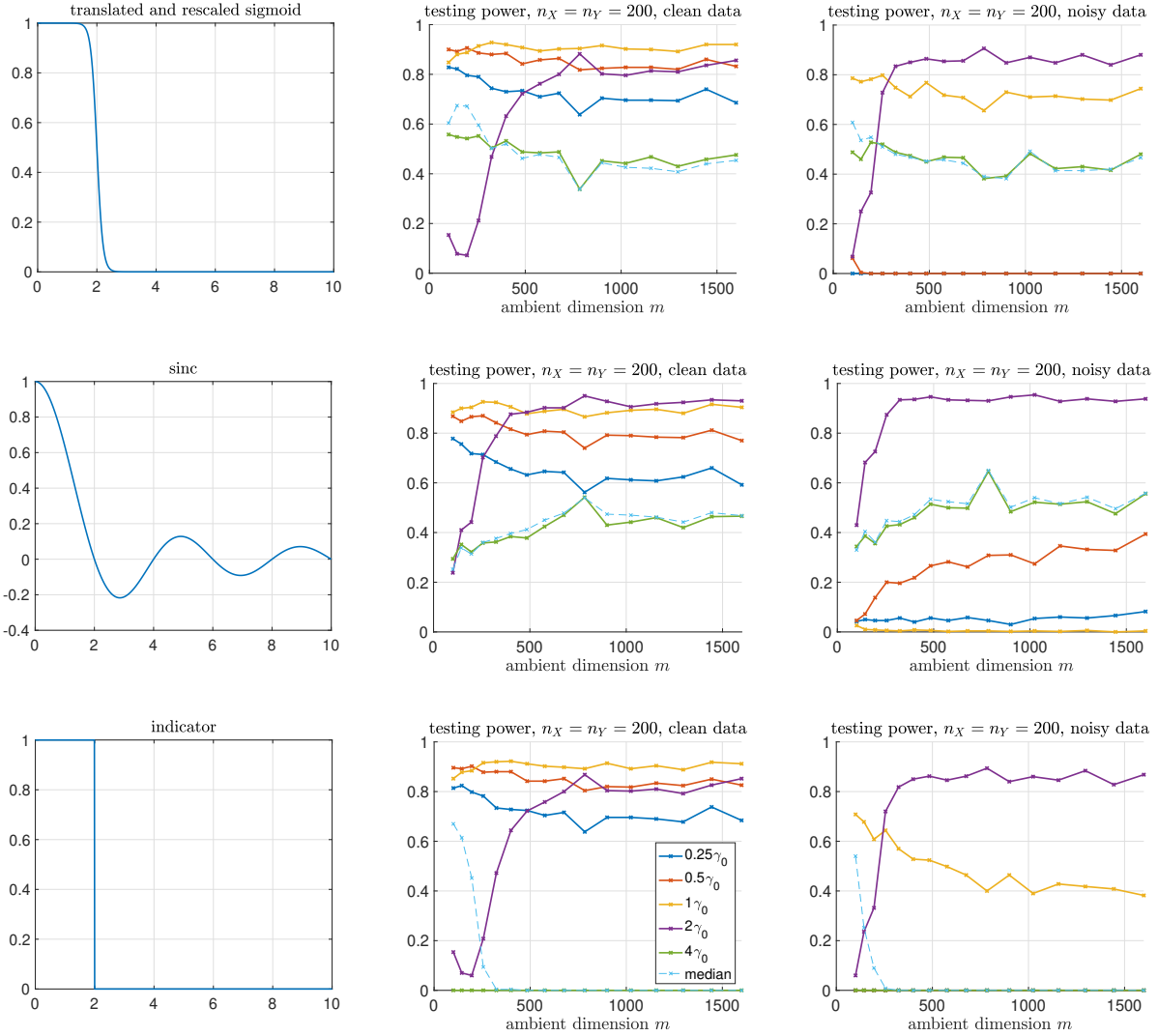


Figure 5: Two-sample test with non-Gaussian kernels that may not be PSD. (Left column) Three choices of kernel function h as in Section 5.3. (Right two columns) Same plots of testing powers on clean and noisy data of rotated images as in Figure 3, of the three kernel functions respectively.

As a remark, unlike in Section 5.1, the MNIST image data do not lie on any constructed manifold induced by latent group action, but only lie near certain manifold-like structures in the ambient space - the latent manifold reveals all possible variations of images of the 10 digits, and since there are 10 classes, there are possibly 10 sub-manifolds (which may be of different intrinsic dimensionalities on each piece), as illustrated by the 2D embedding by tSNE (t-distributed Stochastic Neighbor Embedding [63]) in Figure 4 (Top left). Thus, the case does not fall under the exact theoretical assumption of manifold data in Section 3, even though manifold-like structures are likely to be present in the dataset. The experimental results show that in this generalized case, there may still be a benefit to testing power by using a more localized kernel with a smaller bandwidth than the median distance bandwidth.

5.3 Two-sample tests with non-PSD kernels

Using the same data and experimental set-up as in Section 5.1, we examine different choices of the kernel function h , which are non-Gaussian and possibly non-PSD. The indicator kernel corresponds to the “epsilon-graph” construction frequently used in manifold learning, e.g. in ISOMAP [60]. The example kernels here are mainly designed to verify the theoretical prediction that the test with a non-PSD kernel can still have power, with no suggestion of any immediate practical advantage of these kernels for the testing problems. Specifically, we study

- Sigmoid kernel: $h(r) = \frac{\exp\{-10(r-2)\}}{1+\exp\{-10(r-2)\}}$, which is a translated and rescaled sigmoid function and satisfies Assumption 3.3, but generally gives a non-PSD kernel $K_\gamma(x, y)$ for data in \mathbb{R}^m .
- Sinc kernel: $h(r) = \sin(\frac{\pi}{2}r)/(\frac{\pi}{2}r)$, which takes both positive and negative values on $(0, \infty)$, and only has $1/r$ decay, violating both (C2) and (C3).
- Indicator kernel: $h(r) = \mathbf{1}_{[0,2)}(r)$, which is not continuous on $(0, \infty)$, violating (C1).

Plots of the kernel function $h(r)$ as univariate functions are shown in the left column of Figure 5. The testing power for clean and noisy data over a range of kernel bandwidth, including the median distance bandwidth, are shown in the right two columns (same plots as in Figure 3). The results show that these kernel tests, when the kernel is non-PSD and even violates the theoretical assumption, can obtain testing power if the kernel bandwidth is properly chosen. In addition, the optimal bandwidth may not be the median distance: the best performance achieved by the three kernels for clean data is obtained with γ_0 or $2\gamma_0$ in (21), which is smaller than the median distance as explained in Section 5.1. With noisy data, the testing powers worsen, but the power achieved by the best bandwidth is again comparable to that on the clean data for all three kernels; though the best bandwidth takes a different value from that under the clean data (which can be anticipated based on the analysis in Appendix A.3). Comparing the (translated and rescaled) sigmoid kernel and the indicator kernel in Figure 5, it can be seen that the smoothness of the kernel function leads to better noise robustness; On this data, the Gaussian kernel shows better noise robustness than the non-PSD kernels, comparing Figure 3 with Figure 5.

In all experimental trials presented in this paper, we observe that the testing power remains constant as the dimensionality of the data, denoted by m , increases and ultimately converges. Additionally, our results demonstrate that the curse-of-dimensionality does not affect manifold data and support theoretical proposals that suggest the kernel’s consistency and power in two-sample tests do not depend on whether or not the kernel is PSD, which would result in the test statistic being an RKHS MMD.

6 Discussion

We provide a curse-of-dimensionality free result for kernel MMD-like statistics, which we expect to be tight for the linear-time version of the kernel statistic (see Remark 3.4) but not necessarily for the full (quadratic-time) kernel statistic. For the full kernel statistic computed from data in d -dimensional Euclidean space, [40] showed that the Gaussian kernel statistic achieves a detection rate of $\Delta_2 \gg n^{-4\beta/(d+4\beta)}$, which is minimax optimal against smooth alternatives (c.f. Theorem 5 of [40], recall that Δ_2 is the squared L^2 divergence). One may conjecture the same minimax rate for data with intrinsic data dimension d . This rate of $n^{-4\beta/(d+4\beta)}$ is better than our proved rate of $\Delta_2 \gtrsim n^{-2\beta/(d+4\beta)}$ in Corollary 3.6. This gap may be due to the control of the fluctuation of the U-statistic by Proposition 3.4 not being tight (see the comment after the proposition). Obtaining a test power result at a finite sample size that matches the conjectured minimax rate under our manifold data setting is left to future work. However, the picture differs when considering computational complexity. Since the vanilla computation of the full statistic has $O(n^2)$ complexity, with the same computational and memory cost, the linear-time statistic can process $\tilde{n} \sim n^2$ samples. According to the proved rate by our result, it pushes the detection boundary to be

$\Delta_2 \gtrsim \tilde{n}^{-2\beta/(d+4\beta)} \sim n^{-4\beta/(d+4\beta)}$, which is the same as the conjectured optimal rate. The linear-time statistic can be computed online [26], and thus can be viewed as trading the smaller variance by revisiting all the samples for faster computation on the fly. In summary, the statistical optimality of two-sample kernel statistics applied to intrinsically d -dimensional data remains to be further studied. It would be interesting to design kernel tests that achieve the theoretical detection rate with matched computational complexity.

Our work can be extended in several other directions. For instance, the current paper only considers isotropic kernels with fixed bandwidth. It would be of interest to generalize to other types of kernels used in practice, such as anisotropic kernels using local Mahalanobis distance, other non-Euclidean metrics, kernels with adaptive bandwidth [67, 17], asymmetric kernels with a reference set [36, 16], and so on. To expand the theoretical framework, it would be interesting to go beyond the compactness assumption of the manifold, which would allow extracting the low intrinsic dimensionality or low complexity of high dimensional data distributions that are unbounded or have long tails. One may extend the theory to more complicated manifold structures, like multiple sub-manifolds of different intrinsic dimensions or with complicated boundaries. More advanced analysis of the near-manifold setting, for example, by analyzing general high dimensional noise, would also be a useful extension. Algorithm-wise, while the theory in this work suggests using smaller bandwidth depending on data intrinsic dimensionality and sample size, providing a theoretical scaling of γ for large n , it remains to further develop efficient algorithms to choose kernel bandwidth in practice. Developing efficient kernel testing methods to reduce storage and computational costs would also be desirable. At last, it is natural to extend to other kernel-based testing problems, such as goodness-of-fit tests [19, 35, 56], and general hypothesis tests. Reducing sampling complexity by the intrinsic low-dimensionality of manifold data may also be beneficial therein.

Acknowledgments

The work was supported by NSF DMS-2134037. X.C. was also partially supported by NSF DMS-2237842 and DMS-2007040. Y.X. was also partially supported by an NSF CAREER CCF-1650913, NSF DMS-2134037, CMMI-2015787, CMMI-2112533, DMS-1938106, and DMS-1830210.

References

- [1] Miguel A Arcones and Evarist Gine. On the bootstrap of u and v statistics. *Ann. Statist.*, pages 655–674, 1992.
- [2] Krishnakumar Balasubramanian, Tong Li, and Ming Yuan. On the optimality of kernel-embedding based goodness-of-fit tests. *J. Mach. Learn. Res.*, 22:1–45, 2021.
- [3] Mikhail Belkin and Partha Niyogi. Laplacian eigenmaps for dimensionality reduction and data representation. *Neural Comput.*, 15(6):1373–1396, 2003.
- [4] Mikhail Belkin and Partha Niyogi. Convergence of laplacian eigenmaps. In *Advances in Neural Information Processing Systems*, pages 129–136, 2007.
- [5] Bhaswar B Bhattacharya. Asymptotic distribution and detection thresholds for two-sample tests based on geometric graphs. *Ann. Statist.*, 48(5):2879–2903, 2020.
- [6] Monowar H Bhuyan, Dhruba Kumar Bhattacharyya, and Jugal K Kalita. Network anomaly detection: methods, systems and tools. *IEEE communications surveys & tutorials*, 16(1):303–336, 2013.
- [7] Mikołaj Bińkowski, Danica J. Sutherland, Michael Arbel, and Arthur Gretton. Demystifying MMD GANs. In *International Conference on Learning Representations*, 2018.

- [8] Karsten M Borgwardt, Arthur Gretton, Malte J Rasch, Hans-Peter Kriegel, Bernhard Schölkopf, and Alex J Smola. Integrating structured biological data by kernel maximum mean discrepancy. *Bioinformatics*, 22(14):e49–e57, 2006.
- [9] MR Brito, Adolfo J Quiroz, and Joseph E Yukich. Intrinsic dimension identification via graph-theoretic methods. *J. Multivariate Anal.*, 116:263–277, 2013.
- [10] Antoni Buades, Bartomeu Coll, and J-M Morel. A non-local algorithm for image denoising. In *2005 IEEE Computer Society Conference on Computer Vision and Pattern Recognition (CVPR’05)*, volume 2, pages 60–65. IEEE, 2005.
- [11] Jeff Calder and Nicolas Garcia Trillos. Improved spectral convergence rates for graph Laplacians on ϵ -graphs and k-NN graphs. *Appl. Comput. Harmon. Anal.*, 60:123–175, 2022.
- [12] Yang Cao, Arkadi Nemirovski, Yao Xie, Vincent Guigues, and Anatoli Juditsky. Change detection via affine and quadratic detectors. *Electron. J. Stat.*, 12(1):1–57, 2018.
- [13] Varun Chandola, Arindam Banerjee, and Vipin Kumar. Anomaly detection: A survey. *ACM Comput. Surv.*, 41(3), July 2009.
- [14] Varun Chandola, Arindam Banerjee, and Vipin Kumar. Anomaly detection for discrete sequences: A survey. *IEEE transactions on knowledge and data engineering*, 24(5):823–839, 2010.
- [15] Hao Chen and Jerome H Friedman. A new graph-based two-sample test for multivariate and object data. *J. Amer. Statist. Assoc.*, 112(517):397–409, 2017.
- [16] Xiuyuan Cheng, Alexander Cloninger, and Ronald R Coifman. Two-sample statistics based on anisotropic kernels. *Inf. Inference*, 9(3):677–719, 2020.
- [17] Xiuyuan Cheng and Hau-Tieng Wu. Convergence of graph Laplacian with kNN self-tuned kernels. *Inf. Inference*, 09 2021.
- [18] Xiuyuan Cheng and Nan Wu. Eigen-convergence of gaussian kernelized graph laplacian by manifold heat interpolation. *Appl. Comput. Harmon. Anal.*, 61:132–190, 2022.
- [19] Kacper Chwialkowski, Heiko Strathmann, and Arthur Gretton. A kernel test of goodness of fit. *JMLR: Workshop and Conference Proceedings*, 2016.
- [20] Kacper P Chwialkowski, Aaditya Ramdas, Dino Sejdinovic, and Arthur Gretton. Fast two-sample testing with analytic representations of probability measures. In *Advances in Neural Information Processing Systems*, pages 1981–1989, 2015.
- [21] Ronald R Coifman and Stéphane Lafon. Diffusion maps. *Appl. Comput. Harmon. Anal.*, 21(1):5–30, 2006.
- [22] Eustasio del Barrio, Juan A. Cuesta-Albertos, Carlos Matrán, and Jesús M. Rodríguez-Rodríguez. Tests of goodness of fit based on the l_2 -wasserstein distance. *Ann. Statist.*, 27(4):1230–1239, 08 1999.
- [23] Manfredo Perdigao Do Carmo. *Riemannian geometry*. Springer, 1992.
- [24] David B Dunson, Hau-Tieng Wu, and Nan Wu. Spectral convergence of graph Laplacian and heat kernel reconstruction in L^∞ from random samples. *Appl. Comput. Harmon. Anal.*, 55:282–336, 2021.
- [25] Amir Massoud Farahmand, Csaba Szepesvári, and Jean-Yves Audibert. Manifold-adaptive dimension estimation. In *Proceedings of the 24th international conference on Machine learning*, pages 265–272, 2007.

- [26] Thomas Flynn and Shinjae Yoo. Change detection with the kernel cumulative sum algorithm. In *2019 IEEE 58th Conference on Decision and Control (CDC)*, pages 6092–6099, 2019.
- [27] Arthur Gretton, Karsten M Borgwardt, Malte J Rasch, Bernhard Schölkopf, and Alexander Smola. A kernel two-sample test. *J. Mach. Learn. Res.*, 13(Mar):723–773, 2012.
- [28] Arthur Gretton, Kenji Fukumizu, Zaïd Harchaoui, and Bharath K. Sriperumbudur. A fast, consistent kernel two-sample test. In *Advances in Neural Information Processing Systems 22*, pages 673–681. Curran Associates, Inc., 2009.
- [29] László Györfi and Edward C. Van Der Meulen. *A consistent goodness of fit test based on the total variation distance*, pages 631–645. Springer Netherlands, Dordrecht, 1991.
- [30] Matthias Hein, Jean-Yves Audibert, and Ulrike Von Luxburg. From graphs to manifolds—weak and strong pointwise consistency of graph laplacians. In *International Conference on Computational Learning Theory*, pages 470–485. Springer, 2005.
- [31] James J Higgins. *Introduction to modern nonparametric statistics*. 2003.
- [32] W Hoeffding. Probability inequalities for sums of bounded random variables. *J. Amer. Statist. Assoc.*, 58:13–30, 1963.
- [33] Lajos Horváth and Piotr Kokoszka. *Inference for Functional Data with Applications*. Springer Science & Business Media, 2012.
- [34] Harold Hotelling. The generalization of student’s ratio. *Ann. Math. Statist.*, 2(3):360–378, 08 1931.
- [35] Wittawat Jitkrittum, Heishiro Kanagawa, and Bernhard Schölkopf. Testing goodness of fit of conditional density models with kernels. In *Conference on Uncertainty in Artificial Intelligence*, pages 221–230. PMLR, 2020.
- [36] Wittawat Jitkrittum, Zoltán Szabó, Kacper P Chwialkowski, and Arthur Gretton. Interpretable distribution features with maximum testing power. In *Advances in Neural Information Processing Systems*, pages 181–189, 2016.
- [37] Wittawat Jitkrittum, Wenkai Xu, Zoltán Szabó, Kenji Fukumizu, and Arthur Gretton. A linear-time kernel goodness-of-fit test. In *Advances in Neural Information Processing Systems*, pages 262–271, 2017.
- [38] Elizaveta Levina and Peter Bickel. Maximum likelihood estimation of intrinsic dimension. *Advances in neural information processing systems*, 17, 2004.
- [39] Chun-Liang Li, Wei-Cheng Chang, Yu Cheng, Yiming Yang, and Barnabás Póczos. MMD GAN: Towards deeper understanding of moment matching network. In *Advances in Neural Information Processing Systems*, pages 2203–2213, 2017.
- [40] Tong Li and Ming Yuan. On the optimality of gaussian kernel based nonparametric tests against smooth alternatives. *arXiv preprint arXiv:1909.03302*, 2019.
- [41] James R Lloyd and Zoubin Ghahramani. Statistical model criticism using kernel two sample tests. In *Advances in Neural Information Processing Systems*, pages 829–837, 2015.
- [42] David Lopez-Paz and Maxime Oquab. Revisiting classifier two-sample tests. In *International Conference on Learning Representations*, 2017.

- [43] Frank J Massey. The kolmogorov-smirnov test for goodness of fit. *J. Amer. Statist. Assoc.*, 46(253):68–78, 1951.
- [44] Philippos Mordohai and Gérard Medioni. Dimensionality estimation, manifold learning and function approximation using tensor voting. *J. Mach. Learn. Res.*, 11(1):411–450, 2010.
- [45] Arkadas Ozakin and Alexander G Gray. Submanifold density estimation. In *Advances in Neural Information Processing Systems*, pages 1375–1382, 2009.
- [46] Karl W Pettis, Thomas A Bailey, Anil K Jain, and Richard C Dubes. An intrinsic dimensionality estimator from near-neighbor information. *IEEE Transactions on pattern analysis and machine intelligence*, (1):25–37, 1979.
- [47] Gabriel Peyré. Manifold models for signals and images. *Computer vision and image understanding*, 113(2):249–260, 2009.
- [48] J. Pfanzagl and O. Sheynin. Studies in the history of probability and statistics XLIV A forerunner of the t-distribution. *Biometrika*, 83(4):891–898, 12 1996.
- [49] John W. Pratt and Jean D. Gibbons. *Kolmogorov-Smirnov two-Sample tests*, pages 318–344. Springer New York, New York, NY, 1981.
- [50] Aaditya Ramdas, Nicolás García Trillos, and Marco Cuturi. On wasserstein two-sample testing and related families of nonparametric tests. *Entropy*, 19(2):47, 2017.
- [51] Aaditya Ramdas, Sashank Jakkam Reddi, Barnabás Póczos, Aarti Singh, and Larry Wasserman. On the decreasing power of kernel and distance based nonparametric hypothesis tests in high dimensions. In *Twenty-Ninth AAAI Conference on Artificial Intelligence*, 2015.
- [52] Jie Ren, Peter J Liu, Emily Fertig, Jasper Snoek, Ryan Poplin, Mark Depristo, Joshua Dillon, and Balaji Lakshminarayanan. Likelihood ratios for out-of-distribution detection. *Advances in neural information processing systems*, 32, 2019.
- [53] Wouter Saelens, Robrecht Cannoodt, Helena Todorov, and Yvan Saeys. A comparison of single-cell trajectory inference methods. *Nature biotechnology*, 37(5):547–554, 2019.
- [54] Mark Sandler, Andrew Howard, Menglong Zhu, Andrey Zhmoginov, and Liang-Chieh Chen. Mobilenetv2: Inverted residuals and linear bottlenecks. In *Proceedings of the IEEE Conference on Computer Vision and Pattern Recognition*, pages 4510–4520, 2018.
- [55] Robert J Serfling. *Approximation Theorems of Mathematical Statistics*. John Wiley & Sons, 2009.
- [56] Alexander Shapiro, Yao Xie, and Rui Zhang. Goodness-of-fit tests on manifolds. *IEEE Trans. Inform. Theory*, 67(4):2539–2553, 2021.
- [57] Amit Singer. From graph to manifold laplacian: The convergence rate. *Appl. Comput. Harmon. Anal.*, 21(1):128–134, 2006.
- [58] Bharath K Sriperumbudur, Kenji Fukumizu, Arthur Gretton, Bernhard Schölkopf, Gert RG Lanckriet, et al. On the empirical estimation of integral probability metrics. *Electron. J. Stat.*, 6:1550–1599, 2012.
- [59] Danica J Sutherland, Hsiao-Yu Tung, Heiko Strathmann, Soumyajit De, Aaditya Ramdas, Alex Smola, and Arthur Gretton. Generative models and model criticism via optimized maximum mean discrepancy. In *International Conference on Learning Representations*, 2017.

- [60] Joshua B Tenenbaum, Vin de Silva, and John C Langford. A global geometric framework for nonlinear dimensionality reduction. *Science*, 290(5500):2319–2323, 2000.
- [61] Nicolás García Trillos, Moritz Gerlach, Matthias Hein, and Dejan Slepčev. Error estimates for spectral convergence of the graph laplacian on random geometric graphs toward the laplace–beltrami operator. *Foundations of Computational Mathematics*, 20(4):827–887, 2020.
- [62] Koen Van den Berge, Hector Roux de Bézieux, Kelly Street, Wouter Saelens, Robrecht Cannoodt, Yvan Saeys, Sandrine Dudoit, and Lieven Clement. Trajectory-based differential expression analysis for single-cell sequencing data. *Nature communications*, 11(1):1201, 2020.
- [63] Laurens Van Der Maaten. Accelerating t-sne using tree-based algorithms. *J. Mach. Learn. Res.*, 15(1):3221–3245, 2014.
- [64] George Wynne and Andrew B Duncan. A kernel two-sample test for functional data. *J. Mach. Learn. Res.*, 23(1):3159–3209, 2022.
- [65] Liyan Xie and Yao Xie. Sequential change detection by optimal weighted ℓ_2 divergence. *IEEE Journal on Selected Areas in Information Theory*, 2(2):747–761, 2021.
- [66] Yao Xie and David Siegmund. Sequential multi-sensor change-point detection. *Ann. Statist.*, 41(2):670–692, Apr 2013.
- [67] Lihi Zelnik-Manor and Pietro Perona. Self-tuning spectral clustering. In *Advances in neural information processing systems*, pages 1601–1608, 2005.
- [68] Jun Zhao, Ariel Jaffe, Henry Li, Ofir Lindenbaum, Esen Sefik, Ruaidhrí Jackson, Xiuyuan Cheng, Richard A Flavell, and Yuval Kluger. Detection of differentially abundant cell subpopulations in scrna-seq data. *Proc. Natl. Acad. Sci.*, 118(22), 2021.
- [69] Wei Zhu, Qiang Qiu, Jiaji Huang, Robert Calderbank, Guillermo Sapiro, and Ingrid Daubechies. Ldmnet: Low dimensional manifold regularized neural networks. In *Proceedings of the IEEE Conference on Computer Vision and Pattern Recognition*, pages 2743–2751, 2018.

A Proofs

A.1 Proofs in Section 3

Proof of Lemma 3.1. We denote by $B_r^l(x)$ the Euclidean ball in \mathbb{R}^l of radius $r > 0$ centered at x . When $l = m$, we omit the superscript l and use $B_r(x)$ to denote the Euclidean ball in the ambient space \mathbb{R}^m . In big-O notations, we use subscript $_{MC}$ to emphasize constant dependence on manifold curvature, $_{MV}$ for that on manifold volume, and $_{GM}$ for that on “Gaussian moments” namely the up to the 4-th moments of normal densities in \mathbb{R}^d .

First, we use the sub-exponential decay of h to truncate the integral of $dV(y)$ in (6) on $\mathcal{M} \cap B_{\delta_\gamma}(x)$ only with an $O(\|f\|_\infty \gamma^{10})$ residual, where $\delta_\gamma := \sqrt{\frac{d+10}{a} \gamma^2 \log \frac{1}{\gamma}}$. This is because when $\|y - x\| \geq \delta_\gamma$, by Assumption 3.3(C2), $h(\frac{\|x-y\|^2}{\gamma^2}) \leq e^{-a\delta_\gamma^2/\gamma^2} = \gamma^{d+10}$, and then

$$\begin{aligned} \left| \gamma^{-d} \int_{\mathcal{M} \setminus B_{\delta_\gamma}(x)} h\left(\frac{\|x-y\|^2}{\gamma^2}\right) f(y) dV(y) \right| &\leq \gamma^{-d} \int_{\mathcal{M} \setminus B_{\delta_\gamma}(x)} \gamma^{d+10} |f(y)| dV(y) \\ &\leq \|f\|_\infty \text{Vol}(\mathcal{M}) \gamma^{10} = O_{MV}(\|f\|_\infty \gamma^{10}), \quad \forall x \in \mathcal{M}. \end{aligned} \tag{23}$$

The 10-th power here is only to guarantee that the residual is of a higher order of γ compared to the other residual terms below, and 10 can be made another large constant by increasing the constant factor ‘10’ in the definition of δ_γ accordingly.

Next, we use a local expansion of f and kernel function to compute the integral of $dV(y)$ on $B_{\delta_\gamma}(x)$.

By compactness of \mathcal{M} , there is $\gamma_1(\mathcal{M})$ such that when $\gamma < \gamma_1$ and then δ_γ is sufficiently small, then $B_{\delta_\gamma}(x) \cap \mathcal{M}$ lies inside the geodesic ball of the injective radius of \mathcal{M} and is isomorphic to a ball in \mathbb{R}^d . Then the local chart is well-defined, and we use the local projected coordinate on the tangent plane: Let ϕ_x be the projection to $T_x(\mathcal{M})$, for each $y \in \mathcal{M} \cap B_{\delta_\gamma}(x)$, and define the projected coordinate $u := \phi_x(y - x)$. By the local metric and volume comparisons with respect to the projected coordinate u (see Lemma 6 and 7 in [21], also see Lemma A.1 in [17]), we have

$$\begin{aligned} d_{\mathcal{M}}(x, y) &= \|u\|(1 + O_{MC}(\|u\|^2)), \quad \|y - x\| = \|u\|(1 + O_{MC}(\|u\|^2)), \\ \left| \det \left(\frac{dy}{du} \right) \right| &= 1 + O_{MC}(\|u\|^2), \end{aligned} \quad (24)$$

where the constants are uniform for all x , due to compactness of \mathcal{M} . As a result, (24) implies that there is another $\gamma_2(\mathcal{M})$ such that when $\gamma < \gamma_2$, for any $x \in \mathcal{M}$,

$$\begin{cases} 0.9\|y - x\| \leq 0.9d_{\mathcal{M}}(x, y) \leq \|u\|_{\mathbb{R}^d} \leq \|y - x\| \leq d_{\mathcal{M}}(x, y), \\ \left| \det \left(\frac{dy}{du} \right) \right| \leq 2, \quad \|y - x\|^2 = \|u\|^2 + O_{MC}(\|u\|^4), \end{cases} \quad \forall y \in \mathcal{M} \cap B_{\delta_\gamma}(x). \quad (25)$$

This $\gamma_2(\mathcal{M})$ depends on manifold curvature, and is small when manifold curvature has a large magnitude.

Set $\gamma_0 = \min\{\gamma_1, \gamma_2\}$, when $\gamma < \min\{\gamma_0, 1\}$, we have (24) and (25), where the big-O notation means that the corresponding term has absolute value bounded by the implied constant times the quantity inside the $O(\cdot)$.

We now expand f locally at x , and we separate the two cases, $\beta \leq 1$, and $1 < \beta \leq 2$.

Case 1: $0 < \beta \leq 1$.

Let $y \in B_{\delta_\gamma}(x) \cap \mathcal{M}$, because f has Hölder constant L_f , $|f(y) - f(x)| \leq L_f d_{\mathcal{M}}(x, y)^\beta$. Because locally $d_{\mathcal{M}}(x, y) = O(\|u\|)$ by (24), we have $d_{\mathcal{M}}(x, y)^\beta = O(\|u\|^\beta)$. Thus, with absolute constant in big-O,

$$f(y) = f(x) + O(L_f \|u\|^\beta), \quad \forall y \in \mathcal{M} \cap B_{\delta_\gamma}(x). \quad (26)$$

Meanwhile, by (25) and that h is C^1 on $(0, \infty)$,

$$h\left(\frac{\|x - y\|^2}{\gamma^2}\right) = h\left(\frac{\|u\|^2 + O_{MC}(\|u\|^4)}{\gamma^2}\right) = h\left(\frac{\|u\|^2}{\gamma^2}\right) + h'(\xi(u))O_{MC}\left(\frac{\|u\|^4}{\gamma^2}\right),$$

where $\xi(u)$ is between $\frac{\|u\|^2}{\gamma^2}$ and $\frac{\|x - y\|^2}{\gamma^2}$. By (25), $\xi(u) \geq \frac{\|u\|^2}{\gamma^2}$, and then by Assumption 3.3(C2),

$$|h'(\xi(u))| \leq a_1 e^{-a \frac{\|u\|^2}{\gamma^2}}. \quad (27)$$

Then, we define $B'_x := \phi_x(\mathcal{M} \cap B_{\delta_\gamma}(x)) \subset \mathbb{R}^d$ and have that

$$\begin{aligned} & \gamma^{-d} \int_{\mathcal{M} \cap B_{\delta_\gamma}(x)} h\left(\frac{\|x - y\|^2}{\gamma^2}\right) f(y) dV(y) \\ &= \gamma^{-d} \int_{B'_x} \left(h\left(\frac{\|u\|^2}{\gamma^2}\right) + a_1 e^{-a \frac{\|u\|^2}{\gamma^2}} O_{MC}\left(\frac{\|u\|^4}{\gamma^2}\right) \right) f(y(u)) \left| \det \left(\frac{dy}{du} \right) \right| du \\ &= \gamma^{-d} \int_{B'_x} h\left(\frac{\|u\|^2}{\gamma^2}\right) (f(x) + O(L_f \|u\|^\beta)) \left| \det \left(\frac{dy}{du} \right) \right| du \\ & \quad + \gamma^{-d} \int_{B'_x} a_1 e^{-a \frac{\|u\|^2}{\gamma^2}} O_{MC}\left(\frac{\|u\|^4}{\gamma^2}\right) \|f\|_\infty \left| \det \left(\frac{dy}{du} \right) \right| du = \textcircled{1} + \textcircled{2} + \textcircled{3}, \end{aligned} \quad (28)$$

where, by (24),

$$\textcircled{1} := f(x)\gamma^{-d} \int_{B'_x} h\left(\frac{\|u\|^2}{\gamma^2}\right) (1 + O_{MC}(\|u\|^2)) du,$$

and by (25), $\left|\det\left(\frac{dy}{du}\right)\right| \leq 2$,

$$\textcircled{2} := \gamma^{-d} \int_{B'_x} h\left(\frac{\|u\|^2}{\gamma^2}\right) O(L_f\|u\|^\beta) 2du,$$

$$\textcircled{3} := \gamma^{-d} \int_{B'_x} a_1 e^{-a\frac{\|u\|^2}{\gamma^2}} O_{MC}\left(\frac{\|u\|^4}{\gamma^2}\right) \|f\|_\infty 2du.$$

To proceed, note that B'_x is not a ball on \mathbb{R}^d but is contained between two spheres: by (25), we have $B_{0.9\delta_\gamma}^d(0) \subset B'_x \subset B_{\delta_\gamma}^d(0)$. This together with the exponential decay of h gives that

$$\begin{aligned} \left| \gamma^{-d} \int_{B'_x} h\left(\frac{\|u\|^2}{\gamma^2}\right) du - m_0 \right| &\leq \left| \gamma^{-d} \int_{\mathbb{R}^d \setminus B_{0.9\delta_\gamma}^d(0)} h\left(\frac{\|u\|^2}{\gamma^2}\right) du \right| \\ &\leq \int_{v \in \mathbb{R}^d, \|v\| \geq 0.9\delta_\gamma/\gamma} e^{-a\|v\|^2} dv = O_{GM,a}(\gamma^{10}). \end{aligned}$$

Meanwhile, $\gamma^{-d} \int_{B'_x} h\left(\frac{\|u\|^2}{\gamma^2}\right) \|u\|^2 du = O_{GM,a}(\gamma^2)$. Thus,

$$\textcircled{1} = f(x)(m_0[h] + O_{GM,a}(\gamma^{10}) + O_{GM,a,MC}(\gamma^2)) = m_0 f(x) + O_{GM,a,MC}(\|f\|_\infty \gamma^2).$$

Similarly, $\gamma^{-d} \int_{B'_x} h\left(\frac{\|u\|^2}{\gamma^2}\right) \|u\|^\beta du = O_{GM,a}(\gamma^\beta)$, and then

$$\textcircled{2} = O_{GM,a}(L_f \gamma^\beta).$$

Finally, $\gamma^{-d} \int_{B'_x} e^{-a\frac{\|u\|^2}{\gamma^2}} \frac{\|u\|^4}{\gamma^2} du = O_{GM,a}(\gamma^2)$, and then

$$\textcircled{3} = O_{GM,a,a_1,MC}(\|f\|_\infty \gamma^2).$$

Putting together, we have that (28) equals

$$\textcircled{1} + \textcircled{2} + \textcircled{3} = m_0[h]f(x) + O_{GM,a,a_1,MC}(\|f\|_\infty \gamma^2) + O_{GM,a}(L_f \gamma^\beta),$$

and the integral outside $B_{\delta_\gamma}(x)$ gives $O_{MV}(\|f\|_\infty \gamma^{10})$ as shown in (23). Because $\gamma < 1$, $\gamma^{10} \leq \gamma^2$. Combined together, this proves (6) under case 1 with C_1 being some $C_1^{(\text{case 1})}$, which depends on h (including constants a, a_1), d , and manifold curvature and volume.

Case 2: $1 < \beta \leq 2$.

For $y \in \mathcal{M} \cap B_{\delta_\gamma}(x)$ and thus $d_{\mathcal{M}}(x, y) < \text{inj}(x)$, using the local normal coordinates at x denoted as s , we write $y = \exp_x(s)$, $s \in T_x \mathcal{M}$, and $\|s\| = d_{\mathcal{M}}(x, y)$. The Taylor expansion of f at x gives that

$$f(y) = f(x) + \nabla_{\mathcal{M}} f(x)^T s + O(L'_f \|s\|^\beta), \quad L'_f := \sup_{y \in \mathcal{M}, y \neq x} \|\nabla_{\mathcal{M}} f(x) - \nabla_{\mathcal{M}} f(y)\| / d_{\mathcal{M}}(x, y)^{\beta-1}.$$

Because locally $s = u + O_{MC}(\|u\|^3)$, $\|s\| = O(\|u\|)$, we have

$$f(y) = f(x) + \nabla_{\mathcal{M}} f(x)^T (u + O_{MC}(\|u\|^3)) + O(L'_f \|u\|^\beta).$$

Recall the definition of Hölder constant L_f when $\beta > 1$, we have $\|\nabla_{\mathcal{M}}f(x)\| \|u\|^3 + L'_f \|u\|^\beta = O(L_f \|u\|^\beta)$. As a result, the expansion (26) has the following counterpart for any $y \in \mathcal{M} \cap B_{\delta_\gamma}(x)$,

$$f(y) = f(x) + \nabla_{\mathcal{M}}f(x)^T u + O_{MC}(L_f \|u\|^\beta). \quad (29)$$

Then similarly expanding the kernel $h\left(\frac{\|x-y\|^2}{\gamma^2}\right)$ in the integral, we have

$$\gamma^{-d} \int_{\mathcal{M} \cap B_{\delta_\gamma}(x)} h\left(\frac{\|x-y\|^2}{\gamma^2}\right) f(y) dV(y) = \textcircled{1} + \textcircled{2} + \textcircled{3},$$

where

$$\textcircled{1} := \gamma^{-d} \int_{B'_x} h\left(\frac{\|u\|^2}{\gamma^2}\right) (f(x) + \nabla_{\mathcal{M}}f(x)^T u) (1 + O_{MC}(\|u\|^2)) du,$$

and again, since $\left| \det\left(\frac{dy}{du}\right) \right| \leq 2$,

$$\textcircled{2} := \gamma^{-d} \int_{B'_x} h\left(\frac{\|u\|^2}{\gamma^2}\right) O_{MC}(L_f \|u\|^\beta) 2 du,$$

$$\textcircled{3} := \gamma^{-d} \int_{B'_x} a_1 e^{-a \frac{\|u\|^2}{\gamma^2}} O_{MC}\left(\frac{\|u\|^4}{\gamma^2}\right) \|f\|_\infty 2 du.$$

Same as before, $\textcircled{3} = O_{GM,a,a_1,MC}(\|f\|_\infty \gamma^2)$, and $\textcircled{2} = O_{GM,a,MC}(L_f \gamma^\beta)$. Also, $\textcircled{1} = \textcircled{4} + \textcircled{5}$, where

$$\begin{aligned} \textcircled{4} &= \gamma^{-d} \int_{B'_x} h\left(\frac{\|u\|^2}{\gamma^2}\right) (f(x) + \nabla_{\mathcal{M}}f(x)^T u) du \\ &= m_0 f(x) + f(x) O_{GM,a}(\gamma^{10}) + 0 + \|\nabla_{\mathcal{M}}f(x)\| O_{GM,a}(\gamma^{10}) \\ &= m_0 f(x) + O_{GM,a}((\|f\|_\infty + \|\nabla_{\mathcal{M}}f(x)\|) \gamma^{10}), \end{aligned}$$

where in the 2nd equality we used that the integral of $h\left(\frac{\|u\|^2}{\gamma^2}\right) u du$ vanishes on \mathbb{R}^d ;

$$\begin{aligned} \textcircled{5} &= \gamma^{-d} \int_{B'_x} h\left(\frac{\|u\|^2}{\gamma^2}\right) (f(x) + \nabla_{\mathcal{M}}f(x)^T u) O_{MC}(\|u\|^2) du \\ &= O_{MC,GM,a}(\|f\|_\infty \gamma^2) + O_{MC,GM,a}(\|\nabla_{\mathcal{M}}f\|_\infty \gamma^3). \end{aligned}$$

Putting together, by that $\|\nabla_{\mathcal{M}}f\|_\infty \leq L_f$, we have

$$\textcircled{1} = m_0 [h] f(x) + O_{MC,GM,a}(\|f\|_\infty \gamma^2) + O_{MC,GM,a}(L_f \gamma^3),$$

and thus, since $\gamma^3 \leq \gamma^\beta$,

$$\textcircled{1} + \textcircled{2} + \textcircled{3} = m_0 [h] f(x) + O_{GM,a,MC}(L_f \gamma^\beta) + O_{GM,a,a_1,MC}(\|f\|_\infty \gamma^2).$$

The integral outside $B_{\delta_\gamma}(x)$ again can be incorporated into the residual term above because $\gamma^{10} \leq \gamma^2$. This proves (6) under case 2 with C_1 being some $C_1^{(\text{case } 2)}$ which depends on the kernel function h , d , and manifold curvature and volume.

Choosing $C_1 = \max\{C_1^{(\text{case } 1)}, C_1^{(\text{case } 2)}\}$ makes (6) hold for both cases. \square

Proof of Lemma 3.2. Writing $m_0[h]$ as m_0 for abbreviation. For any $x \in \mathcal{M}$, applying Lemma 3.1 to when $f = p - q$ gives that

$$\begin{aligned} \gamma^{-d} \int_{\mathcal{M}} K_\gamma(x, y)(p - q)(y)dV(y) &= m_0(p - q)(x) + r_1(x), \\ \text{where } r_1 \text{ satisfies } \|r_1\|_\infty &\leq 2C_1(L_\rho\gamma^\beta + \rho_{\max}\gamma^2), \end{aligned} \quad (30)$$

where $L_f \leq 2L_\rho$ and $\|f\|_\infty \leq 2\rho_{\max}$ due to that $L_p, L_q \leq L_\rho$ and $\|p\|_\infty, \|q\|_\infty \leq \rho_{\max}$ by Assumption 3.2. Then,

$$\begin{aligned} \gamma^{-d}T &= \int_{\mathcal{M}} \left(\gamma^{-d} \int_{\mathcal{M}} K_\gamma(x, y)(p - q)(y)dV(y) \right) (p - q)(x)dV(x) \\ &= \int_{\mathcal{M}} (m_0(p - q) + r_1) (p - q)dV \\ &= m_0\Delta_2 + r_T, \end{aligned}$$

where r_T has the expression

$$r_T = \int_{\mathcal{M}} r_1(p - q)dV.$$

By Cauchy-Schwarz,

$$\begin{aligned} |r_T| &\leq \left(\int_{\mathcal{M}} |r_1|^2 dV \right)^{1/2} \left(\int_{\mathcal{M}} (p - q)^2 dV \right)^{1/2} \\ &\leq \|r_1\|_\infty \text{Vol}(\mathcal{M})^{1/2} \Delta_2^{1/2}. \end{aligned}$$

Together with the bound of $\|r_1\|_\infty$ in (30) this gives

$$|r_T| \leq 2C_1 \text{Vol}(\mathcal{M})^{1/2} (L_\rho\gamma^\beta + \rho_{\max}\gamma^2) \Delta_2^{1/2},$$

which proves (9) by that $0 < \beta \leq 2$, $0 < \gamma < 1$, and the definition of \tilde{C}_1 as in the lemma. \square

Proof of Proposition 3.4. By definition,

$$\hat{T} = \hat{T}_{XX} + \hat{T}_{YY} - 2\hat{T}_{XY},$$

where

$$\hat{T}_{XX} = \frac{1}{n_X^2} \sum_{i, i'=1}^{n_X} K_\gamma(x_i, x_{i'}), \quad \hat{T}_{YY} = \frac{1}{n_Y^2} \sum_{j, j'=1}^{n_Y} K_\gamma(y_j, y_{j'}), \quad \hat{T}_{XY} = \frac{1}{n_X n_Y} \sum_{i=1}^{n_X} \sum_{j=1}^{n_Y} K_\gamma(x_i, y_j),$$

and we analyze the concentration of the three terms respectively. By (11),

$$n_X - 1 \geq 0.9\rho_X n, \quad n_Y - 1 \geq 0.9(1 - \rho_X)n,$$

and thus by definition of c as in (12),

$$cn \leq n_X - 1, \quad n_Y - 1 \leq n. \quad (31)$$

We first analyze \hat{T}_{XX} . Since $K_\gamma(x, x) = h(0)$,

$$\hat{T}_{XX} = \frac{h(0)}{n_X} + \left(1 - \frac{1}{n_X}\right) V_{XX}, \quad V_{XX} := \frac{1}{n_X(n_X - 1)} \sum_{i \neq j, i, j=1}^{n_X} K_\gamma(x_i, x_j).$$

We write $n_X = N$ for a short-handed notation. Define, for $i \neq j$, $V_{ij} := K_\gamma(x_i, x_j)$, we have that

$$\mathbb{E}V_{i,j} = \mathbb{E}_{x \sim p, y \sim p} K_\gamma(x, y).$$

Meanwhile, by that $|h(r)| \leq 1 =: L_V$ for any $r \in [0, \infty)$, due to Assumption 3.3 (C2), we always have $|V_{ij}| \leq L_V$. This boundedness of V_{ij} will be used in the Bernstein-type argument below. The variance

$$\text{Var}(V_{ij}) \leq \mathbb{E}V_{ij}^2 = \int_{\mathcal{M}} \int_{\mathcal{M}} h^2 \left(\frac{\|x - y\|^2}{\gamma^2} \right) p(x)p(y) dV(x) dV(y).$$

Note that $h_2 := h^2$ also satisfies Assumption 3.3 (with constants a being replaced by $2a$, same $a_0 = 1$ and a_1 replaced by $2a_1$), and thus one can apply Lemma 3.1 with h replaced by h_2 , which does not change the threshold constant γ_0 , but the constant C_1 in the error bound changes to $C_1^{(2)}$ corresponding to the new kernel function h_2 . Since $\gamma < \min\{1, \gamma_0\}$, applying Lemma 3.1 with h_2 and $f = 1$ gives that

$$\left| \gamma^{-d} \int_{\mathcal{M}} h^2 \left(\frac{\|x - y\|^2}{\gamma^2} \right) dV(y) - m_0[h^2] \right| \leq C_1^{(2)} \gamma^2.$$

Thus

$$\begin{aligned} \mathbb{E}V_{ij}^2 &\leq \gamma^d \|p\|_\infty \int_{\mathcal{M}} p(x) \left(m_0[h^2] + C_1^{(2)} \gamma^2 \right) dV(x) \\ &\leq \gamma^d \rho_{\max} \left(m_0[h^2] + C_1^{(2)} \gamma^2 \right), \end{aligned} \quad (32)$$

Since we assume $\gamma < \frac{1}{\sqrt{C_1^{(2)}}}$ in the condition, by definition of ν as in (12), we then have that

$$\text{Var}(V_{ij}) \leq \gamma^d \nu. \quad (33)$$

We use the decoupling of U-statistics: Define $\tilde{V}_{i,j} = V_{ij} - \mathbb{E}V_{ij}$ for $i \neq j$. For any $s > 0$, let \mathcal{S}_N be denote the permutation group of N elements, we have

$$\begin{aligned} V_{XX} - \mathbb{E}V_{ij} &= \frac{1}{N(N-1)} \sum_{i \neq j} \tilde{V}_{i,j} = \frac{1}{N!} \frac{1}{N(N-1)} \sum_{\gamma \in \mathcal{S}_N} \sum_{i \neq j} \tilde{V}_{\gamma(i), \gamma(j)} \\ &= \frac{1}{N!} \frac{1}{\lfloor N/2 \rfloor} \sum_{\gamma \in \mathcal{S}_N} \sum_{i=1}^{\lfloor N/2 \rfloor} \tilde{V}_{\gamma(2i-1), \gamma(2i)}. \end{aligned}$$

Then, by Jensen's inequality, let $M = \lfloor N/2 \rfloor$,

$$\mathbb{E}e^{s(V_{XX} - \mathbb{E}V_{ij})} \leq \frac{1}{N!} \sum_{\gamma \in \mathcal{S}_N} \mathbb{E} \exp \left\{ s \frac{1}{M} \sum_{i=1}^M \tilde{V}_{\gamma(2i-1), \gamma(2i)} \right\} = \mathbb{E} \exp \left\{ s \frac{1}{M} \sum_{i=1}^M \tilde{V}_{2i-1, 2i} \right\},$$

and the sum over i is an independent sum over M random variables. By that $|\tilde{V}_{ij}| \leq 1$, and (33), then same as in the derivation of the classical Bernstein's inequality, we have that for any $t > 0$,

$$\mathbb{P}[V_{XX} - \mathbb{E}V_{ij} > t] \leq \exp \left\{ -\frac{\lfloor N/2 \rfloor t^2}{2\gamma^d \nu + \frac{2}{3} t L_V} \right\} \leq \exp \left\{ -\frac{(N-1)t^2}{2(2\gamma^d \nu + \frac{2}{3} t L_V)} \right\}.$$

We target at

$$t = \lambda \sqrt{\frac{\gamma^d \nu}{N-1}}, \quad \lambda > 0,$$

and when

$$\frac{tL_V}{3} < \gamma^d \nu, \quad (34)$$

the tail probability is bounded by

$$\exp\left\{-\frac{(N-1)t^2}{8\gamma^d \nu}\right\} = \exp\left\{-\frac{\lambda^2}{8}\right\}.$$

By that $L_V = 1$, the requirement (34) is equivalent to $\lambda\sqrt{\frac{\gamma^d \nu}{N-1}} < 3\gamma^d \nu$ which is

$$0 < \lambda < 3\sqrt{\nu\gamma^d(N-1)}.$$

This proves that

$$\mathbb{P}\left[V_{XX} - \mathbb{E}V_{ij} > \lambda\sqrt{\frac{\gamma^d \nu}{(N-1)}}\right] \leq e^{-\lambda^2/8}, \quad \forall 0 < \lambda < 3\sqrt{\nu\gamma^d(N-1)}. \quad (35)$$

The lower-tail can be proved similarly. So we have

$$\mathbb{P}\left[V_{XX} - \mathbb{E}_{x \sim p, y \sim p} K_\gamma(x, y) > \lambda\sqrt{\frac{\gamma^d \nu}{n_X - 1}}\right] \leq e^{-\lambda^2/8}, \quad \forall 0 < \lambda < 3\sqrt{\nu\gamma^d(n_X - 1)}, \quad (36)$$

and same for $\mathbb{P}\left[V_{XX} - \mathbb{E}_{x \sim p, y \sim p} K_\gamma(x, y) < -\lambda\sqrt{\frac{\gamma^d \nu}{n_X - 1}}\right]$.

Similarly, we have

$$\widehat{T}_{YY} = \frac{h(0)}{n_Y} + \left(1 - \frac{1}{n_Y}\right)V_{YY}, \quad V_{YY} := \frac{1}{n_Y(n_Y - 1)} \sum_{i \neq j, i, j=1}^{n_Y} K_\gamma(y_i, y_j).$$

and

$$\mathbb{P}\left[V_{YY} - \mathbb{E}_{x \sim q, y \sim q} K_\gamma(x, y) > \lambda\sqrt{\frac{\gamma^d \nu}{n_Y - 1}}\right] \leq e^{-\lambda^2/8}, \quad \forall 0 < \lambda < 3\sqrt{\nu\gamma^d(n_Y - 1)}, \quad (37)$$

and same for $\mathbb{P}\left[V_{YY} - \mathbb{E}_{x \sim q, y \sim q} K_\gamma(x, y) < -\lambda\sqrt{\frac{\gamma^d \nu}{n_Y - 1}}\right]$.

To analyze \widehat{T}_{XY} , define $M := \min\{n_X, n_Y\}$, and

$$\widetilde{V}_{i,j} = K_\gamma(x_i, y_j) - \mathbb{E}_{x \sim p, y \sim q} K_\gamma(x, y), \quad i = 1, \dots, n_X, j = 1, \dots, n_Y.$$

Then for any $s > 0$, let \mathcal{S}_X and \mathcal{S}_Y denote the permutation group of n_X and n_Y elements respectively, we then have

$$\begin{aligned} \frac{1}{n_X n_Y} \sum_{i=1}^{n_X} \sum_{j=1}^{n_Y} \widetilde{V}_{i,j} &= \frac{1}{n_X!} \frac{1}{n_Y!} \frac{1}{n_X n_Y} \sum_{\gamma_X \in \mathcal{S}_X} \sum_{\gamma_Y \in \mathcal{S}_Y} \sum_{i=1}^{n_X} \sum_{j=1}^{n_Y} \widetilde{V}_{\gamma_X(i), \gamma_Y(j)} \\ &= \frac{1}{n_X!} \frac{1}{n_Y!} \frac{1}{M} \sum_{\gamma_X \in \mathcal{S}_X} \sum_{\gamma_Y \in \mathcal{S}_Y} \sum_{i=1}^M \widetilde{V}_{\gamma_X(i), \gamma_Y(i)}. \end{aligned}$$

Then, by Jensen's inequality,

$$\begin{aligned} \mathbb{E} \exp \left\{ s \frac{1}{n_X n_Y} \sum_{i=1}^{n_X} \sum_{j=1}^{n_Y} \tilde{V}_{i,j} \right\} &\leq \frac{1}{n_X! n_Y!} \sum_{\gamma_X \in \mathcal{S}_X} \sum_{\gamma_Y \in \mathcal{S}_Y} \mathbb{E} \exp \left\{ s \frac{1}{M} \sum_{i=1}^M \tilde{V}_{\gamma_X(i), \gamma_Y(i)} \right\} \\ &= \mathbb{E} \exp \left\{ s \frac{1}{M} \sum_{i=1}^M \tilde{V}_{i,i} \right\}, \end{aligned}$$

and $\tilde{V}_{i,i} = K_\gamma(x_i, y_i) - \mathbb{E} K_\gamma(x_i, y_i)$ across $i = 1, \dots, M$ are independent. By that $|\tilde{V}_{ij}| \leq 1$, and same as before, by applying Lemma 3.1 with h^2 and use that $\gamma < \frac{1}{\sqrt{C_1^{(2)}}}$,

$$\text{Var}(\tilde{V}_{ij}) \leq \mathbb{E} V_{ij}^2 = \int_{\mathcal{M}} \int_{\mathcal{M}} h^2 \left(\frac{\|x-y\|^2}{\gamma^2} \right) p(x)q(y) dV(x) dV(y) \leq \gamma^{d\nu},$$

then same as in proving (35), we have

$$\mathbb{P} \left[\hat{T}_{XY} - \mathbb{E}_{x \sim p, y \sim q} K_\gamma(x, y) > \lambda \sqrt{\frac{\gamma^{d\nu}}{M}} \right] \leq e^{-\lambda^2/8}, \quad \forall 0 < \lambda < 3\sqrt{\nu \gamma^d M}, \quad (38)$$

and same for $\mathbb{P} \left[\hat{T}_{XY} - \mathbb{E}_{x \sim p, y \sim q} K_\gamma(x, y) < -\lambda \sqrt{\frac{\gamma^{d\nu}}{M}} \right]$.

Recall that

$$\hat{T} = (V_{XX} + V_{YY} - 2\hat{T}_{XY}) + \frac{1}{n_X} (h(0) - V_{XX}) + \frac{1}{n_Y} (h(0) - V_{YY}),$$

we now collect (36)(37)(38) to derive concentration of \hat{T} around T :

Upper tail. by Assumption 3.3(C2)(C3), $h(0) - V_{XX} \leq h(0) \leq 1$, and similarly for $h(0) - V_{YY}$, and then

$$\hat{T} \leq V_{XX} + V_{YY} - 2\hat{T}_{XY} + \left(\frac{1}{n_X} + \frac{1}{n_Y} \right).$$

Recall that

$$\begin{aligned} \mathbb{E} V_{XX} + V_{YY} - 2\hat{T}_{XY} \\ = (\mathbb{E}_{x \sim p, y \sim p} + \mathbb{E}_{x \sim q, y \sim q} - 2\mathbb{E}_{x \sim p, y \sim q}) K_\gamma(x, y) = T. \end{aligned}$$

Applying upper tail bounds in (36)(37)(38), together with that $n_X - 1, n_Y - 1 \geq cn$ by (31), we have that for any $\lambda < 3\sqrt{c\nu\gamma^d n}$, with probability $\geq 1 - 3e^{-\lambda^2/8}$,

$$\hat{T} \leq T + \frac{2}{cn} + 4\lambda \sqrt{\frac{\gamma^{d\nu}}{cn}},$$

Lower tail. Because $h(0) - V_{XX} \geq -V_{XX} \geq -1$, and similarly for $h(0) - V_{YY}$,

$$\hat{T} \geq V_{XX} + V_{YY} - 2\hat{T}_{XY} - \left(\frac{1}{n_X} + \frac{1}{n_Y} \right).$$

The lower tail bound is then proved similarly using the lower tail bounds in (36)(37)(38). \square

Proof of Theorem 3.5. Under the condition of the theorem, the conditions needed by Proposition 3.4 and Lemma 3.2 are both satisfied. We first verify that the Type-I error is at most α_{level} . The definition of

λ_1 makes that $3e^{-\lambda_1^2/8} = \alpha_{\text{level}}$. Under H_0 , we have $T = 0$ because $p = q$. The upper tail bound in Proposition 3.4 gives that for any $0 < \lambda < 3\sqrt{c\nu\gamma^d n}$,

$$\widehat{T} \leq \frac{2}{cn} + 4\lambda\sqrt{\frac{\nu\gamma^d}{c n}}, \quad \text{with probability } \geq 1 - 3e^{-\lambda^2/8}. \quad (39)$$

By the definition of t_{thres} , (39) implies that the type-I error bound holds as long as $\lambda_1 < 3\sqrt{c\nu\gamma^d n}$, and this is guaranteed by (14).

Next, we address the Type-II error. By the lower tail bound in Proposition 3.4, the Type-II error bound $3e^{-\lambda_2^2/8}$ holds as long as $\lambda_2 < 3\sqrt{c\nu\gamma^d n}$ and

$$t_{\text{thres}} < T - 4\lambda_2\sqrt{\frac{\nu\gamma^d}{c n} - \frac{2}{cn}}, \quad (40)$$

which we are to prove here: Define $D_{p,q} := m_0[h]\Delta_2$. By Lemma 3.2, $T = \gamma^d(D_{p,q} + r_T)$, and $|r_T| \leq \tilde{C}_1(L_\rho + \rho_{\max})\gamma^\beta\Delta_2^{1/2}$. By (13), we have

$$|r_T| < 0.1m_0[h]\Delta_2 = 0.1D_{p,q},$$

and then $T > \gamma^d 0.9D_{p,q}$. Meanwhile, (14) gives that

$$\frac{4}{cn} < 0.4\gamma^d D_{p,q}, \quad 4(\lambda_1 + \lambda_2)\sqrt{\frac{\nu\gamma^d}{c n}} < 0.5\gamma^d D_{p,q}. \quad (41)$$

Thus,

$$\frac{4}{cn} + 4(\lambda_1 + \lambda_2)\sqrt{\frac{\nu\gamma^d}{c n}} < 0.9\gamma^d D_{p,q} < T,$$

which implies (40) by the constructive choice of t_{thres} as in the theorem. \square

Proof of Corollary 3.6. To apply Theorem 3.5 and notations as therein, recall that

$$\lambda_1 = \sqrt{8\log(3/\alpha_{\text{level}})},$$

and we define $\lambda_2 := \sqrt{8\log(3/\epsilon)}$. Then, by (15), we have the Type-II error $\mathbb{P}[\widehat{T} \leq t_{\text{thres}} | H_1] \leq \epsilon$ if all the needed conditions in Theorem 3.5, including (13) and (14), can be satisfied.

The condition (13) and the requirement $\gamma < \tilde{\gamma}_1 := \min\{1, \gamma_0, (C_1^{(2)})^{-1/2}\}$ in Theorem 3.5 will be satisfied if

$$\gamma^\beta < c_1\Delta_2^{1/2} \quad \text{and} \quad \gamma < \tilde{\gamma}_1, \quad (42)$$

where the positive constant c_1 depends on (L_ρ, ρ_{\max}) and (\mathcal{M}, h) , and $\tilde{\gamma}_1$ is determined by (\mathcal{M}, h) .

As for the condition (14), first note that when Δ_2 is smaller than an $O(1)$ constant d_2 , which only depends on $m_0[h]$ and ν , the third term will dominate the right hand side of (14), and here we used that $\lambda_1 + \lambda_2 \geq \lambda_1 > \sqrt{8\log 6}$. Since the dominating term scales as $(\lambda_1 + \lambda_2)^2/\Delta_2^2$, the condition (14) can be satisfied if

$$\Delta_2^2 > c_2 \left(\log \frac{1}{\alpha_{\text{level}}} + \log \frac{1}{\epsilon} \right) \gamma^{-d} n^{-1}, \quad (43)$$

where the positive constant c_2 depends on ρ_{\max} , ρ_X and (\mathcal{M}, h) .

Assuming $\Delta_2 < d_2$, and by definition, the constant d_2 is determined by h , d , and ρ_{\max} . To finish the proof of the $(1 - \epsilon)$ power, it suffices to show that under the stated scaling of γ and (16), the needed conditions (42) and (43) can be fulfilled at large n .

Now recall that we have $\gamma \sim n^{-1/(d+4\beta)}$. To satisfy (42), first, we have $\gamma < \tilde{\gamma}_1$ for large n ; There is also a positive constant c_5 (only depending on β) such that $\gamma^\beta < c_5 n^{-\beta/(d+4\beta)}$ for large n . As a result, (42) can be satisfied if

$$c_5 n^{-\beta/(d+4\beta)} < c_1 \Delta_2^{1/2}.$$

Comparing to (16), using the relation that $\log \frac{1}{\alpha_{\text{level}}} + \log \frac{1}{\epsilon} \geq \log \frac{1}{\alpha_{\text{level}}} > \log 2$, we have that (16) can fulfill (42) as long as c_3 satisfies that

$$c_3 (\log 2)^{1/2} > (c_5/c_1)^2. \quad (44)$$

To satisfy (43), note that there is a positive constant c_4 (only depending on d) such that, for large n , $\gamma^d > c_4 n^{-d/(d+4\beta)}$. Then, the condition (43) can be satisfied if

$$\Delta_2^2 > (c_2/c_4) \left(\log \frac{1}{\alpha_{\text{level}}} + \log \frac{1}{\epsilon} \right) n^{-4\beta/(d+4\beta)}.$$

Comparing to (16), we know that this can be fulfilled if

$$c_3 > (c_2/c_4)^{1/2}. \quad (45)$$

Collecting (44) and (45), we can define c_3 to be a positive constant to satisfy both and the dependence of c_3 is as stated in the corollary. As a result, all the needed conditions in Theorem 3.5 for (15) to hold are satisfied at large n , which proves the test level and that the test power is at least $1 - \epsilon$.

Finally, consider when $\Delta_2 \gg n^{-2\beta/(d+4\beta)}$. Note that the Type-II error is non-negative and the above argument shows that for any small ϵ , the requirement (16) will hold eventually. This proves that test power will approach to 1 as n increases. \square

A.2 Proofs in Section 4.1

Proof of Lemma 4.1. The proof uses same technique as Lemma 3.1 and the handling of x near boundary follows the method of Lemma 9 in [21].

The constant γ'_0 is defined similarly as before, to guarantee the existence of local chart at point x both away from and near boundary (including the uniqueness of the Euclidean distance nearest point $x_0 \in \partial\mathcal{M}$ to each x when $d_E(x, \partial\mathcal{M}) \leq \delta_\gamma$), along with the local metric and volume comparison after using projected coordinates u as (24) and (25). The existence of such γ'_0 is due to compactness of \mathcal{M} .

For x satisfying $d_E(x, \partial\mathcal{M}) > \delta_\gamma$, the analysis is the same as in the proof of Lemma 3.1 by truncating the integral of $dV(y)$ on $B_{\delta_\gamma}(x) \cap \mathcal{M}$. We thus have (6) hold at x with the constant C_1 as therein.

To analyze the case for x where $d_E(x, \partial\mathcal{M}) \leq \delta_\gamma$, let $x_0 \in \partial\mathcal{M}$ be the nearest point on the boundary to x under Euclidean distance, and we follow the same change of coordinates around x_0 as in the proof of Lemma 9 in [21]. For $0 < \beta \leq 1$, by the symmetry of the kernel $h(\frac{\|u\|^2}{\gamma^2})$ and the same analysis in Lemma 9 of [21], one can show that

$$\begin{aligned} \gamma^{-d} \int_{B_{\delta_\gamma}(x) \cap \mathcal{M}} h\left(\frac{\|x-y\|^2}{\gamma^2}\right) f(y) dV(y) &= f(x) m_0^{(\gamma)}[h](x) \\ &+ O_{GM,a}(L_f \gamma^\beta) + O_{GM,a,a_1,MC}(\|f\|_\infty \gamma^2), \end{aligned} \quad (46)$$

where $m_0^{(\gamma)}[h](x)$ equals the integral of $\gamma^{-d} h(\frac{\|u\|^2}{\gamma^2})$ on a partial domain in \mathbb{R}^d and the domain depends on the location of x , defined in the same way as in Lemma 9 in [21], and it satisfies that $m_0^{(\gamma)}[h](x) \leq m_0[h]$ due to that $h \geq 0$ by Assumption 3.3 (C3). The $O_{GM,a}(L_f \gamma^\beta)$ term is due to the expansion of f near x , and the $O_{GM,a,a_1,MC}(\|f\|_\infty \gamma^2)$ due to the expansion of kernel and the volume form $|\det(\frac{dy}{du})| = 1 + O(\|u\|^2)$, similar as in the proof of Lemma 3.1. When $1 < \beta \leq 2$, f is C^1 but there is an $O(\|\nabla_{\mathcal{M}} f\|_\infty \gamma)$ residual

term in the expansion of (46) due to that the integral of $h(\|u\|^2/\gamma^2)u$ on part of \mathbb{R}^d no longer vanishes. As a result, the term $O_{GM,a}(L_f\gamma^\beta)$ becomes $O_{GM,a}(L_f\gamma)$ and dominates the $O(\gamma^\beta)$ term. Putting together, this proves (17) with the bound $C'_1(L_f\gamma^{\beta\wedge 1} + \|f\|_\infty\gamma^2)$ on the r.h.s., where C'_1 is a constant depending on (\mathcal{M}, h) . \square

Proof of Lemma 4.2. Recall the definition of constant δ_γ be as in Lemma 4.1. Omit $[h]$ in the notation of constant $m_0[h]$ and function $m_0^{(\gamma)}[h](x)$ for abbreviation. Applying Lemma 4.1 to $f = p - q$, where $L_f \leq 2L_\rho$ and $\|f\|_\infty \leq 2\rho_{\max}$ same as in the proof of Lemma 3.2, we have that

(i) For any $x \in \mathcal{M} \setminus P_\gamma$,

$$\begin{aligned} \gamma^{-d} \int_{\mathcal{M}} K_\gamma(x, y)(p - q)(y)dV(y) &= m_0(p - q)(x) + r_1(x), \\ \text{where } r_1 \text{ satisfies } \sup_{x \in \mathcal{M} \setminus P_\gamma} |r_1(x)| &\leq 2C_1(L_\rho\gamma^\beta + \rho_{\max}\gamma^2) \leq 2C_1(L_\rho + \rho_{\max})\gamma^\beta. \end{aligned} \quad (47)$$

(ii) For any $x \in P_\gamma$,

$$\begin{aligned} \gamma^{-d} \int_{\mathcal{M}} K_\gamma(x, y)(p - q)(y)dV(y) &= m_0^{(\gamma)}(x)(p - q)(x) + r_2(x), \\ \text{where } r_2 \text{ satisfies } \sup_{x \in P_\gamma} |r_2(x)| &\leq 2C'_1(L_\rho\gamma^{\beta\wedge 1} + \rho_{\max}\gamma^2) \leq 2C'_1(L_\rho + \rho_{\max})\gamma^{\beta\wedge 1}. \end{aligned} \quad (48)$$

Then,

$$\begin{aligned} \gamma^{-d}T &= \left(\int_{\mathcal{M} \setminus P_\gamma} + \int_{P_\gamma} \right) \left(\gamma^{-d} \int_{\mathcal{M}} K_\gamma(x, y)(p - q)(y)dV(y) \right) (p - q)(x)dV(x) \\ &= \int_{\mathcal{M} \setminus P_\gamma} (m_0(p - q) + r_1)(p - q)dV + \int_{P_\gamma} (m_0^{(\gamma)}(p - q) + r_2)(p - q)dV, \\ &= \int (m_0\mathbf{1}_{\mathcal{M} \setminus P_\gamma} + m_0^{(\gamma)}\mathbf{1}_{P_\gamma})(p - q)^2dV + \int (r_1\mathbf{1}_{\mathcal{M} \setminus P_\gamma} + r_2\mathbf{1}_{P_\gamma})(p - q)dV, \end{aligned}$$

which gives that

$$\begin{aligned} r_T &= \gamma^{-d}T - m_0\Delta_2 \\ &= \int_{P_\gamma} (m_0^{(\gamma)} - m_0)(p - q)^2dV + \int_{\mathcal{M} \setminus P_\gamma} r_1(p - q)dV + \int_{P_\gamma} r_2(p - q)dV \\ &=: \textcircled{1} + \textcircled{2} + \textcircled{3}. \end{aligned} \quad (49)$$

To bound each of the three terms respectively, first, by that $0 \leq m_0^{(\gamma)}(x) \leq m_0$ for all $x \in P_\gamma$, we have

$$|\textcircled{1}| \leq m_0 \int_{P_\gamma} (p - q)^2dV \leq m_0C_3\delta_\gamma\Delta_2, \quad (50)$$

where the second inequality is by Assumption 4.2. Next, by Cauchy-Schwarz,

$$\begin{aligned} |\textcircled{2}| &\leq \left(\int_{\mathcal{M} \setminus P_\gamma} |r_1|^2dV \right)^{1/2} \left(\int_{\mathcal{M} \setminus P_\gamma} (p - q)^2dV \right)^{1/2} \\ &\leq 2C_1(L_\rho + \rho_{\max})\gamma^\beta \text{Vol}(\mathcal{M})^{1/2}\Delta_2^{1/2}, \end{aligned} \quad (51)$$

where we used the uniform upper bound of $|r_1(x)|$ as in (47). By that $\tilde{C}_1 = 2C_1 \text{Vol}(\mathcal{M})^{1/2}$ as defined in Lemma 3.2, this gives

$$|\textcircled{2}| \leq \tilde{C}_1 (L_\rho + \rho_{\max}) \gamma^\beta \Delta_2^{1/2}. \quad (52)$$

Similarly, by (48) and Assumption 4.2,

$$\begin{aligned} |\textcircled{3}| &\leq \left(\int_{P_\gamma} |r_2|^2 dV \right)^{1/2} \left(\int_{P_\gamma} (p-q)^2 dV \right)^{1/2} \\ &\leq 2C'_1 (L_\rho + \rho_{\max}) \gamma^{\beta \wedge 1} \left(\int_{P_\gamma} dV \right)^{1/2} (C_3 \delta_\gamma \Delta_2)^{1/2}. \end{aligned} \quad (53)$$

The volume of the domain P_γ can be shown to be upper bounded by $\int_{P_\gamma} dV \leq c_2 \delta_\gamma |\partial\mathcal{M}|$ for some constant c_2 depending on the curvature of \mathcal{M} and the regularity of $\partial\mathcal{M}$. Then (53) continues as

$$|\textcircled{3}| \leq 2C'_1 (c_2 C_3)^{1/2} |\partial\mathcal{M}|^{1/2} (L_\rho + \rho_{\max}) \gamma^{\beta \wedge 1} \delta_\gamma \Delta_2^{1/2}.$$

Define $\tilde{C}'_2 := 2C'_1 (c_2 C_3)^{1/2} |\partial\mathcal{M}|^{1/2}$, we have

$$|\textcircled{3}| \leq \tilde{C}'_2 (L_\rho + \rho_{\max}) \gamma^{\beta \wedge 1} \delta_\gamma \Delta_2^{1/2}. \quad (54)$$

Collecting (50)(52)(54) and inserting back to (49) proves (18) by triangle inequality, where the constants \tilde{C}_1 and \tilde{C}'_2 are as stated in the lemma. \square

Proof of Theorem 4.3. We first extend Proposition 3.4, and it suffices to bound the integral

$$\mathbb{E}_{x \sim p, y \sim p} K_\gamma(x, y)^2 \leq \nu \gamma^d, \quad (55)$$

where ν is defined as in (12), and the same for $\mathbb{E}_{x \sim q, y \sim q} K_\gamma(x, y)^2$ and $\mathbb{E}_{x \sim p, y \sim q} K_\gamma(x, y)^2$. We prove in below that this is the case when $\gamma < (C_1^{(2)})^{-1/2}$, where $C_1^{(2)}$ corresponds to the constant C'_1 in Lemma 4.1 replacing h with h^2 , and thus $C_1^{(2)}$ only depends on (\mathcal{M}, h) . Then the same deviation bounds as in Proposition 3.4 can be proved after replacing the constants $C_1^{(2)}$ with $C_1^{(2)}$, and γ_0 with γ'_0 , in the statement.

The rest of the proof of Theorem 3.5 applies here. Specifically, the Type-I error bound is guaranteed by the choice of t_{thres} , and the Type-II error bound holds as long as

$$|r_T| < 0.1 m_0 [h] \Delta_2. \quad (56)$$

By Lemma 4.2, (56) follows from (18) under the condition (19).

To finish the proof, it remains to show (55) when $\gamma < (C_1^{(2)})^{-1/2}$ and the same for

$$\mathbb{E}_{x \sim q, y \sim q} K_\gamma(x, y)^2 \quad \text{and} \quad \mathbb{E}_{x \sim p, y \sim q} K_\gamma(x, y)^2.$$

To prove this, similarly as in the proof of Proposition 3.4, by considering $h_2 = h^2$ as the kernel function we have

$$\mathbb{E}_{x \sim p, y \sim p} K_\gamma(x, y)^2 \leq \int_{\mathcal{M}} p(x) \rho_{\max} \left(\int_{\mathcal{M}} K_\gamma(x, y)^2 dV(y) \right) dV(x). \quad (57)$$

Applying Lemma 4.1 with h replaced by h^2 and $f = 1$ gives that

$$\gamma^{-d} \int_{\mathcal{M}} K_\gamma(x, y)^2 dV(y) = \begin{cases} m_0 [h^2] + r_2(x), & x \in \mathcal{M} \setminus P_\gamma \\ m_0^{(\gamma)} [h^2](x) + r_2(x), & x \in P_\gamma \end{cases}$$

where

$$\sup_{x \in \mathcal{M}} |r_2(x)| \leq C_1'^{(2)} \gamma^2,$$

and the constant $C_1'^{(2)}$ equals the maximum of C_1 and C_1' in Lemma 4.1 corresponding to the kernel function h^2 , which then depends on (\mathcal{M}, h) only. By that $m_0^{(\gamma)}[h^2](x) \leq m_0[h^2]$, this gives that

$$\int_{\mathcal{M}} K_\gamma(x, y)^2 dV(y) \leq \gamma^d \left(m_0[h^2] + C_1'^{(2)} \gamma^2 \right), \quad \forall x \in \mathcal{M}.$$

Inserting back to (57), we have

$$\mathbb{E}_{x \sim p, y \sim p} K_\gamma(x, y)^2 \leq \rho_{\max} \gamma^d \left(m_0[h^2] + C_1'^{(2)} \gamma^2 \right),$$

which is bounded by $\gamma^d \nu$ when $C_1'^{(2)} \gamma^2 < 1$. This argument from (57) applies in the same way to $\mathbb{E}_{x \sim q, y \sim q} K_\gamma(x, y)^2$ and $\mathbb{E}_{x \sim p, y \sim q} K_\gamma(x, y)^2$, and then they observe the same upper-bound as in (55). \square

A.3 Proofs in Section 4.2

Recall that with Gaussian additive noise in \mathbb{R}^m , the law of x_i and y_i can be written as, for $k = 1, 2$,

$$x_i = x_i^{(c)} + \xi_i^{(1)}, \quad y_j = y_j^{(c)} + \xi_j^{(2)}, \quad x_i^{(c)} \sim p_{\mathcal{M}}, \quad y_j^{(c)} \sim q_{\mathcal{M}}, \quad \xi_i^{(k)} \sim \mathcal{N}(0, \sigma_{(k)}^2 I_m),$$

where $x_i^{(c)}, y_j^{(c)}, \xi_i^{(1)}$ and $\xi_i^{(2)}$ are independent, and $p_{\mathcal{M}}$ and $q_{\mathcal{M}}$ are manifold data densities supported on \mathcal{M} and satisfy Assumption 3.2. We want to show that our theory in Section 3 extends to this case when h is Gaussian kernel and the noise level $\sigma := \sqrt{\sigma_{(1)}^2 + \sigma_{(2)}^2} \leq \frac{c}{\sqrt{m}} \gamma$ for some constant c .

Though p and q are now supported on the ambient space, by the form of p and q and $h(\xi) = e^{-\xi^2/2}$, we have that

$$\begin{aligned} & \int_{\mathbb{R}^m} \int_{\mathbb{R}^m} K_\gamma(x, y) p(x) p(y) dx dy \\ &= \int_{\mathcal{M}} \int_{\mathcal{M}} \mathbb{E}_{\xi, \eta} \exp \left\{ -\frac{\|(x_1 + \xi) - (y_1 + \eta)\|^2}{2\gamma^2} \right\} p_{\mathcal{M}}(x_1) p_{\mathcal{M}}(y_1) dx_1 dy_1 \\ &= \int_{\mathcal{M}} \int_{\mathcal{M}} \mathbb{E}_g \exp \left\{ -\frac{\|(x_1 - y_1)/\gamma + g\|^2}{2} \right\} p_{\mathcal{M}}(x_1) p_{\mathcal{M}}(y_1) dx_1 dy_1, \quad g \sim \mathcal{N} \left(0, \frac{\sigma^2}{\gamma^2} I_m \right). \end{aligned}$$

Define $\tilde{\sigma}^2 := \frac{\sigma^2}{\gamma^2}$, we have that for any vector $v \in \mathbb{R}^m$,

$$\mathbb{E}_g \exp \left\{ -\frac{\|v + g\|^2}{2} \right\} = \frac{1}{(1 + \tilde{\sigma}^2)^{m/2}} \exp \left\{ -\frac{\|v\|^2}{2(1 + \tilde{\sigma}^2)} \right\},$$

thus $\int_{\mathbb{R}^m} \int_{\mathbb{R}^m} K_\gamma(x, y) p(x) p(y) dx dy$ can be equivalently written as

$$\int_{\mathcal{M}} \int_{\mathcal{M}} \frac{1}{(1 + \tilde{\sigma}^2)^{m/2}} \exp \left\{ -\frac{\|x_1 - y_1\|^2}{2\gamma^2(1 + \tilde{\sigma}^2)} \right\} p_{\mathcal{M}}(x_1) p_{\mathcal{M}}(y_1) dx_1 dy_1. \quad (58)$$

Because $h(\xi)^2 = e^{-\xi^2}$, the integral of $K_\gamma(x, y)^2$ can be computed similarly and it gives

$$\begin{aligned} & \int_{\mathbb{R}^m} \int_{\mathbb{R}^m} K_\gamma(x, y)^2 p(x) p(y) dx dy \\ &= \int_{\mathcal{M}} \int_{\mathcal{M}} \mathbb{E}_{\xi, \eta} \exp \left\{ -\frac{\|(x_1 + \xi) - (y_1 + \eta)\|^2}{\gamma^2} \right\} p_{\mathcal{M}}(x_1) p_{\mathcal{M}}(y_1) dx_1 dy_1 \\ &= \int_{\mathcal{M}} \int_{\mathcal{M}} \frac{1}{(1 + 2\tilde{\sigma}^2)^{m/2}} \exp \left\{ -\frac{\|x_1 - y_1\|^2}{\gamma^2(1 + 2\tilde{\sigma}^2)} \right\} p_{\mathcal{M}}(x_1) p_{\mathcal{M}}(y_1) dx_1 dy_1. \end{aligned} \quad (59)$$

Since $\sigma \leq \frac{c}{\sqrt{m}}\gamma$, $\tilde{\sigma}^2 \leq \frac{1}{m}c^2$, and then $1 \leq (1 + \tilde{\sigma}^2)^{m/2} \leq (1 + \frac{c^2}{m})^{m/2} \leq \exp\{c^2/2\}$, which means that the normalizing constant in (58) is bounded to be $O(1)$ constant. The same holds for that normalizing constant in (59), namely $1 \leq (1 + 2\tilde{\sigma}^2)^{m/2} \leq \exp\{c^2\}$.

This means that one can apply Lemma 3.1 to compute the integrals in (58) and (59), replacing the p and q in the lemma by $p_{\mathcal{M}}$ and $q_{\mathcal{M}}$ respectively. We define the new effective kernel bandwidths in the Gaussian kernel: $\tilde{\gamma}^{(1)} := \gamma\sqrt{1 + \tilde{\sigma}^2}$ for integral of $K_{\gamma}(x, y)$ and $\tilde{\gamma}^{(2)} := \gamma\sqrt{1 + 2\tilde{\sigma}^2}$ for that of $K_{\gamma}(x, y)^2$. Since $\tilde{\sigma}^2 \leq c^2/m$, when m is large, the ratios of $\tilde{\gamma}^{(1)}/\gamma$ and $\tilde{\gamma}^{(2)}/\gamma$ are bounded to be $1 + O(m^{-1})$ and thus both ratios are ~ 1 . This implies the approximate expression of T in Lemma 3.2 involving $\Delta_2(p_{\mathcal{M}}, q_{\mathcal{M}})$, as well as the boundedness of variance of $K_{\gamma}(x_i, x_j)$ (and $K_{\gamma}(y_i, y_j)$, $K_{\gamma}(x_i, y_j)$) needed in Proposition 3.4, replacing p and q with $p_{\mathcal{M}}$ and $q_{\mathcal{M}}$, and γ with the new effective kernel bandwidths in the analysis. These replacements allows to prove the same result as in Theorem 3.5 (the constants L_{ρ} and ρ_{\max} are with respect to $p_{\mathcal{M}}$ and $q_{\mathcal{M}}$), where the constants in the bounds need to be adjusted by multiplying some absolute ones.

B Algorithm and bootstrap estimation of t_{thres}

In experiments of kernel two-sample tests, we use the vanilla $O(n^2)$ algorithm to construct the kernel matrix from datasets X and Y and then compute the value of \hat{T} . The summary of the algorithm is as follows

Input data: X and Y , each having n_X and n_Y samples

Parameters: kernel bandwidth γ , test threshold t_{thres} if available.

Step 1. Construct the n -by- n kernel matrix, $n = n_X + n_Y$,

$$K = \begin{bmatrix} K_{XX}, K_{XY} \\ K_{XY}^T, K_{YY} \end{bmatrix},$$

where $K_{XX} = (K_{\gamma}(x_i, x_j))_{1 \leq i, j \leq n_X}$, $K_{YY} = (K_{\gamma}(y_i, y_j))_{1 \leq i, j \leq n_Y}$, and $K_{XY} = (K_{\gamma}(x_i, y_j))_{1 \leq i \leq n_X, 1 \leq j \leq n_Y}$.

Step 2. Compute \hat{T} as defined in (2) from the kernel matrix K .

Step 3. If $\hat{T} < t_{\text{thres}}$, accept $H_0 : p = q$, otherwise, reject H_0 .

If the test threshold t_{thres} is not provided, we use the bootstrap procedure [1] (previously used in [27, 51]) to estimate it from data: Given the computed kernel matrix K , and target test level α_{level} ,

Step 4. Repeating $l = 1, \dots, n_{\text{boot}}$ times:

- Randomly permute the rows and columns of K simultaneously, obtain a matrix K_l
- Compute the statistic \hat{T}_l from K_l , treating the first n_X rows and columns are from one dataset and the other n_Y rows and columns from another data set.

Step 5. From the empirical distribution of n_{boot} , evaluate the $(1 - \alpha_{\text{level}})$ -quantile as t_{thres} .

Note that in the bootstrap procedure for threshold evaluation, no re-computing of the kernel matrix K is needed, but only the block average over the n^2 entries according to the permuted two sample class labels.

The testing power is estimated by n_{run} random replicas of the experiments and counts the frequency that the test is correctly rejected when $q \neq p$. In our experiments, we use n_{boot} and n_{run} a few hundred in our experiments.